

Diagenetic dissolution, maghemitization and sulphidization of magnetic minerals in rapidly deposited gas hydrate bearing sediments from the Bay of Bengal.

Firoz Badesab^{1*}, Virsen Gaikwad^{1,2}, M. Venkateshwarlu³, N. Kadam^{1,2}, Hilda Maria João¹

¹ CSIR - National Institute of Oceanography, Dona Paula-403004, Goa, India

²School of Earth Ocean and Atmospheric sciences, Goa University 403206, Goa, India

³CSIR–National Geophysical Research Institute, Uppal Road, Hyderabad 500007, India

*Corresponding author: Dr. Firoz Badesab (firoz@nio.org)

Abstract

We conducted a comprehensive rock magnetic investigation complemented by a scanning electron microscopy analyses on a 148.8 m sediment core (NGHP-01-20A) from the methane-hydrate bearing site in the Bay of Bengal to systematically evaluate how magnetic minerals selectively respond to a range of diagenetic processes in the sulfidic and methanic sediments. For diagenetic analysis, we defined five distinct sediment magnetic zones (I-V) based on the sediment magnetic signatures. Rock magnetic property is mainly carried by complex magnetic mineral assemblages of detrital (titanomagnetite, silicate hosted magnetic inclusions), altered (titanomaghemite, titanohematite) and fine-grained diagenetic (pyrite) and authigenic (greigite) iron sulfide minerals. Three distinct bands of enhanced magnetic susceptibility in Z-II, Z-III and Z-V mainly comprised of detrital magnetite-rich minerals delivered by the peninsular river systems as a result of higher sedimentation events in the Krishna-Godavari (K-G) basin. Progressive diagenetic dissolution of primary iron oxide and consequent formation of iron sulfide in the uppermost sulfidic zone (Z-I) is clearly mirrored in the magnetic susceptibility (χ_{lf}) profile. Presence of moderately altered coarse-grained detrital Fe-Ti particles in the deeper methanic and magnetically enhanced zones (Z-II, Z-III, Z-V) suggest that sediment diagenesis at this site was significantly constrained by the multiple events of rapid sedimentation which might have restricted the complete dissolution of the primary minerals. Decline in magnetic grain size diagnostic proxy (ARM/IRM_{2.5T}) in the uppermost sulfidic zones (Z-I, Z-II) can be attributed to the preferential dissolution of fine-grained magnetite. Further, downcore increases could be linked with the authigenic formation of fine-grained magnetite in methanic zones (Z-III to Z-V). Ferrimagnetic iron sulfide (greigite) indicative (SIRM/ χ_{lf}) parameter showed sudden rise in Z-II and remain fairly constant throughout, suggesting the presence of authigenic greigite. Scanning electron microscopy in-line with energy dispersive X-ray spectroscopy analyses of magnetic particles from different sediment magnetic zones revealed a range of ferrimagnetic (titanomagnetite, titanomaghemite), antiferromagnetic (titanohematite) iron oxides and iron sulfide (pyrite). Detrital titanomagnetite with angular, irregular, spherical and well-defined octahedral with micron and submicron sized particles mainly derived from Deccan Volcanic Province (DVP) dominates the rock magnetic signal of bulk sediments in the studied core. We noticed several evidence of diagenetic dissolution, sulphidization and maghemitization of magnetic particles in the studied sediment core. Few nanometre-sized detrital magnetic particles occur as inclusions within the silicate minerals and remains protected against the sulfidic dissolution fronts through geologic times. Optical microscopy revealed the dominance of diagenetic pyrite occurring as overgrowth on the ferrimagnetic particles. We demonstrate that the rockmagnetic methods in combination with focussed electron microscope analyses provide valuable insights into the mineralogy, genesis and state of preservation of magnetic particles in sulfidic and methanic environments and thereby enhances the interpretative value of rock magnetic proxies.

1. Introduction

Magnetic minerals are sensitive to sedimentary redox conditions and effectively record the diagenetic effects ranging from subtle to pervasive through geologic time (Canfield, 1989; Roberts, 2015). Magnetic mineral diagenesis in oxic environments incorporate surface oxidation and precipitation of Fe^{3+} bearing minerals from solution. In anoxic environments, the detrital iron mineral undergoes dissolution and releases Fe^{2+} which is readily available for diagenetic reactions (Jørgensen et al., 2004; Liu et al., 2012; Raiswell & Canfield, 2012). Anaerobic oxidation of methane (AOM) is a vital biogeochemical process that results from the interaction of rising methane flux and downward diffusing sulfate concentration (Treude et al., 2005; Knittel & Boetius, 2009). AOM is achieved by a syntrophic consortium of methane oxidizing archaea and sulfate reducing bacteria (Boetius et al., 2000). Organoclastic sulfate reduction (OSR) coupled with AOM process produces large amounts of hydrogen sulfide into pore waters of the host sediment (Canfield & Berner, 1987; Riedinger et al., 2005). In sulphidic environment, iron-bearing minerals undergo severe diagenetic alterations. Dissolved Fe^{2+} released from detrital iron oxides reacts with dissolved hydrogen sulfide produce during OSR and AOM to form sedimentary iron sulphides, mainly pyrite (Berner, 1984; Canfield & Berner, 1987; Roberts & Turner, 1993; Neretin et al., 2004; Rowan et al., 2009; Johnson et al., 2021). Such processes gives rise to consumption of pore-water methane and sulfate to depletion and this zone is widely recognized as sulfate-methane transition zone (SMTZ). Several researchers have successfully established the linkage between distinct minima and maxima in the sediment magnetic susceptibility at SMTZ with the dissolution of magnetite and secondary formation of paramagnetic pyrite and intermediate ferrimagnetic greigite respectively (Garming et al., 2005; Riedinger et al., 2005; Larrasoña et al., 2007; Roberts, 2015; Badesab et al., 2019).

Sedimentation can significantly influence the diagenesis and authigenesis of magnetic minerals in methanic/marine sediments (Borowski et al., 1996; Kasten et al., 2003; Garming et al., 2005; Riedinger et al., 2005; Roberts, 2015; Kars et al., 2021; Koster et al., 2021). The rate of magnetite dissolution is strongly dependent on the sedimentation rate, sulfate reduction rate, concentration of dissolved sulphide and the contact time between the magnetic particles and sulphidic pore-fluids (Roberts & Turner, 1993; Channell & Stoner, 2002; Riedinger et al., 2005; Amiel et al., 2020). Rapid burial of magnetic particles due to increased sediment supply restrict the production of pore-water sulphide and thereby enhances the preservation magnetic particles (Kao et al., 2004; Kawamura et al., 2007; Kars et al., 2014). For example, uniform sediment supply and reactive organic matter will drive steady-state diagenetic reactions towards completion resulting in a significant loss of iron-bearing minerals through subsequent conversion into paramagnetic iron

sulfides. Such mineral transformations can be easily tracked using magnetic proxies (Roberts & Weaver, 2005; Roberts, 2015; Reilly et al., 2020). Contrastingly, non-steady diagenesis arise when sedimentation supply changes rapidly through geologic time and the diagenetic reactions gets significantly affected resulting in complex pattern of magnetic mineral assemblages (Roberts et al., 1996; Ao et al., 2010; Nowaczyk, 2011). For example, mass transport deposits in the continental slope of the K-G basin, Bay of Bengal were generated as a result of slumping/sliding events triggered by the rapid sedimentation, gas hydrate dissociation and neotectonic events (Ramana et al., 2007; Dewangan et al., 2008; Ramprasad et al., 2011; Joao et al., 2021). Rockmagnetic studies on the sediment cores from active and relict cold seep (Gaikwad et al., 2021), shallow gas hydrate (Dewangan et al., 2013; Badesab et al., 2019; Badesab et al., 2020), and deep-seated gas hydrate sites (NGHP-01-10D, NGHP-01-03B, NGHP-01-05C, NGHP-01-7B; NGHP-01-14A Fig. 1; Badesab et al., 2017; 2019; 2020a) in the Bay of Bengal highlighted the impact of mass transport deposits (MTD's) on the gas hydrate related biogeochemical processes and the evolution of complex magnetic mineralogies at these sites.

Diagenesis and authigenesis of magnetic minerals in an active, relict cold seeps and gas hydrate bearing sediments has been extensively studied worldwide. For example, K-G basin, Bay of Bengal (Dewangan et al., 2013; Badesab et al., 2017, 2019, 2020; Gaikwad et al., 2021; Johnson et al., 2021), Nankai Trough, Japan (Kars & Kodama 2015a,b; Musgrave et al., 2019), Cascadia Margin, offshore Oregon (Musgrave,1996; Novosel et al., 2005; Housen & Larrasoña et al., 2007; Esteban et al., 2008), offshore western Svalbard (Johnson et al., 2014; Panieri et al., 2016), Continental margin off Argentina and Uruguay (Riedinger et al., 2005), and Yungan Ridge, offshore southwestern Taiwan (Horng, C.S. 2018). More recently, Johnson et al. (2021) developed a new approach based on heavy mineral proxy and X-ray fluorescence (Zr/Rb) data for isolating the detrital and diagenetic signals in methanic sediments from the K-G basin. Impact of low and high temperature diagenesis on magnetic mineral assemblages in methane hydrate bearing marine sediments from the Nankai Trough was investigated by Kars et al (2018, 2021). Their work revealed that changes in sediment input and organic matter supply, burial temperature and tectonic fluid circulation through geologic time constrained the sediment magnetic signals. Evolution of long term changes in the biogeochemical processes and the associated diagenetic overprinting of the primary magnetic mineral assemblages in the Nankai trough offshore Japan was reconstructed using rock magnetic, solid phase and porewater data (Koster et al., 2021). In similar context, a focussed rock magnetic study by Musgrave et al. (2019) on a 1,800m long sediment sequence in a volcano-

bounded basin on the Izu rear arc, Japan clearly demonstrated how episodes of multiple fluid inputs and pyritization processes controlled the progressive and punctuated magnetic mineral diagenesis.

Despite of extensive environmental and rock magnetic research focussing on understanding magnetic mineral diagenesis in the marine gas hydrate sedimentary system, there is no systematic study till date which examines how magnetic minerals selectively respond to a range of diagenetic processes in the sulfidic and methanic environments respectively. The K-G basin is characterized by a highly dynamic depositional (high sedimentation rates, shale-tectonism, active cold seeps, shallow and deep-seated gas hydrates) conditions and represents a suitable sedimentary environment to study geological and geochemical controls on the magnetic mineral diagenesis. The sediment core (NGHP-01-20A) retrieved from the region prone to high sedimentation in the K-G basin provided a suitable environment to investigate how range of diagenetic processes in the sulfidic and methanic conditions modify the sediment magnetic signals. In the present study, we investigate a 148.8 m long sediment core (NGHP-01-20A) retrieved from the K-G basin during the first Indian National Gas Hydrate Drilling Expedition (NGHP-Exp-01) which offered an excellent opportunity to evaluate the impact of progressive diagenetic dissolution, maghemitization, and sulphidization of detrital magnetic particles on the sediment rock magnetic properties in the marine gas hydrate system using rock magnetic method. A comprehensive SEM-EDS analyses has been employed to systematically visualize the mechanisms of diagenetic alterations and selective response of magnetic particles in the sulfidic and methanic sediments. For site selection, our assessment regarding impact of detrital sedimentation and diagenesis on the rock magnetic sediment record of the core NGHP-01-20A is based on the recent findings of Johnson et al (2021) which successfully isolated the detrital and diagenetic signals based on the good correlation between Zr/Rb and χ records of methane-bearing marine sediment cores. The studied sites (NGHP-01-16A, NGHP-01-10D; Johnson et al., 2021) are proximal to the core location (NGHP-01-20A; present study) in the K-G basin, Bay of Bengal.

2. Study Area, Core Location and Geological Setting

Drilling, logging and coring activities under the aegis of India's first National Gas Hydrate Program (NGHP) confirmed the presence of sub-surface gas hydrate deposits in the K-G basin (Collett et al., 2008). Site NGHP-01-20 (15° 48.5671' N, 81°50.5760' E) lies on the continental slope of the K-G basin (Fig.1). A 148.8 m long drilled sediment core NGHP-01-20A was retrieved onboard DV JOIDES Resolution from the Site NGHP-01-20 in the water depth of ~ 1146 m (Fig. 1). Based on the physical and sedimentological properties, the entire recovered sedimentary sequence of NGHP-01-20A was classified as one lithostratigraphy unit. Sediment lithology mainly comprised of nanofossil-bearing to -rich clay, volcanic glass-bearing to -rich clay, pyrite-bearing to -rich clay,

and authigenic carbonate-bearing to -rich clay sediments (Collet et al., 2008). Various sand and silt beds, laminations were noticed at this site. Shell fragments, foraminifera and methane-derived authigenic carbonates (bands, nodules, tubes, cement) occur throughout the core. The mineralogy composed of iron-rich carbonate and low-magnesium calcite (LMC) (Teichert et al., 2014). Disseminated-type methane hydrate with low saturation at site NGHP-01-20A was found to occur in the fine-grained sediments as confirmed through pore-water chloride (48 to 118 mbsf) and temperature (~ 43 mbsf and 115 to 125 mbsf) anomalies (Collett et al., 2008). The SMTZ depth at this site is ~ 15 mbsf, which is at shallowest depth compared to other drilled sites in the K-G basin, except at site NGHP-01-03C and NGHP-01-05C where the SMTZ depth is at ~ 9 mbsf and ~10 mbsf respectively. Total organic carbon (TOC) content ranges from 0.65 to 2.2 wt.% and CaCO₃ ranges from 0.27 to 12.62 wt%, with the highest values of TOC found between 42 to 92 mbsf (Johnson et al., 2014). The clay mineralogy at this site is dominated by high content of smectite (50 % to 76%) with considerable kaolinite (9 % to 21 %), and illite (3 to 24%) content (Phillips et al., 2014). Influence of high sedimentation events on the pore water geochemical profiles of core NGHP-01-20A has been studied using kinetic modelling approach (Hong et al., 2014).

The K-G basin is a proven petroliferous basin situated in the central part of the eastern continental margin of India (ECMI) (Fig. 1). Sediment thicknesses of about 3–5 km in the onshore region and 8 km in the offshore region have been reported (Prabhakar & Zutshi, 1993; Bastia, 2007). The Holocene-Pleistocene sedimentary deposits in the K-G basin are governed by smectite-bearing Godavari clay formations (Rao, 2001). The annual sediment transport of the Krishna and Godavari rivers is estimated around 67.7 and 170×10^6 t, respectively (Biksham & Subramanian, 1988; Ramesh & Subramanian, 1988). Bulk of the detrital sediment load to the basin is delivered by the Krishna and Godavari river systems which drains through the Deccan Traps, Dharwar and Bastar cratons, and hinterlands of the Godavari graben and Eastern Ghats belt. Detrital iron oxide minerals are ubiquitous in these source rocks (Biksham & Subramanian, 1988; Mazumdar et al., 2015; Johnson et al., 2021). The sediment rock magnetic properties in the K-G basin is carried by the ferrimagnetic detrital titanomagnetites derived from the proximal basalts of DVP (Ramesh & Subramanian, 1988; Sangode et al., 2007).

3. Sampling and measurements

A 148.8 m long sediment core (NGHP-01-20A) was collected using conventional coring systems including the Advanced Piston Corer (APC) and the Extended Core Barrel (XCB). These systems collect sediment cores of approximately 9.6 m long with a diameter of 6.7 cm in a transparent polycarbonate core liners. Sub-sampling was carried out at the intervals of 1.5 to 6 m on

each 9.6 m long section of sediment core (NGHP-01-20A). The sediment core sub samples were later transported and further stored at $\sim 5 - 6$ °C at the cold repository of CSIR-National Institute of Oceanography, Goa, India. For rock magnetic analyses, sediment sub samples of core NGHP-01-20A were dried, weighed, packed in a 25-mm cylindrical sample bottles. The sub samples were later measured for mass-dependent magnetic susceptibility. We compared the shipboard multi-sensor core logger (MSCL) derived magnetic susceptibility (in 2006; Collet et al., 2008) to the laboratory based mass-specific magnetic susceptibility (in January - 2021). We observed minimum alteration to the magnetic signals after core collection and storage (Fig. S7). Magnetic susceptibility and remanence measurements were carried out at the paleomagnetic laboratory of Council of Scientific and Industrial Research-National Institute of Oceanography (CSIR-NIO), Goa, India. Specialized rock magnetic measurements including thermomagnetic and hysteresis loop were conducted on the selected sediment samples at the paleomagnetic Laboratory of CSIR-National Geophysical Research Institute (NGRI), Hyderabad, India.

3.1. Rock magnetic analyses

Low-field low frequency (0.47 kHz) magnetic susceptibility (χ) was measured on sediment samples using a MS2B Bartington Instruments magnetic susceptibility meter. Anhysteretic remanent magnetization (ARM) was imparted using a 100 mT Molspin alternating field (AF) with a superimposed fixed direct current (DC) bias field of 50 μ T with pARM attachment and the remanent magnetism was measured using an AGICO JR-6A automatic spinner magnetometer. An isothermal remanent magnetization (IRM) was imparted in an inducing field of +2.5 T in the forward direction and was demagnetized by DC backfields at -20 mT, - 30 mT, - 100 mT, and - 300 mT using a MMPM10 pulse magnetizer. The corresponding remanences were measured using AGICO JR-6A automatic spinner magnetometer. Titanomagnetite is the dominant magnetic mineral and governed the rock magnetic sediment record of the K-G basin (Sangode et al., 2007; Dewangan et al., 2013; Badesab et al., 2017, 2019; 2020; Johnson et al., 2021). Considering this, we have therefore considered the mass-normalized IRM acquired at a peak field of +2.5T as the saturation isothermal remanent magnetization (SIRM). S-ratio was estimated following the Bloemendal et al. (1992) formulae: $S_{-0.3T} = (IRM_{-300mT}/IRM_{2.5T})$. Temperature-dependent magnetization curves and the hysteresis loop analyses on selected sediment samples were conducted using Advanced Variable Field Translation Balance (AVFTB) housed at the paleomagnetic Laboratory of CSIR-NGRI, Hyderabad, India.

3.2. Magnetic Mineral Extraction, SEM-EDS analyses and optical microscopy

About 5 g of bulk sediment samples were disintegrated into 500 ml of distilled water. For better dispersion, we added 200 mg of sodium hexametaphosphate and suspensions were further treated with ultrasonics. The sediment slurry was allowed to pass through the magnetic extraction unit (Petersen et al., 1986) continuously for 4 – 5 hrs. Separation of magnetic particles is based on the principle that high magnetic field gradients are generated by loading magnets on the teflon coated iron finger. During the circulation process, the magnetic particles within the bulk sediments get attracted towards the iron finger. These particles are further removed and washed multiple times to remove the fine clay fractions. A scanning electron microscope (JEOL JSM-5800 LV) was used to capture the images of the magnetic particles in a secondary electron (SE) imaging mode at energy levels between 15 and 20 kV. The composition of magnetic particles was determined using an energy dispersive X - ray spectroscopy (EDS) probe attached to the microscope. Optical microscopy on separated >63 μm fraction from different sediment intervals was conducted on Nikon SMZ 18 Stereo Zoom Microscope.

3.3. Geochemical Data

Total organic carbon (TOC) and calcium carbonate (CaCO_3) content of the studied sediment core (NGHP-01-20A) was taken from Johnson et al (2014). Pore-water sulfate, alkalinity and gas (methane) data presented in this study are from Collett et al (2008).

4. Results

4.1. Rock magnetic and geochemical properties of sediment core NGHP-01-20A

Five distinct sediment magnetic zones (Z-I to Z-V) were defined based on the down-core variations in χ_{lf} and SIRM (Fig. 2). A trend of downcore reduction in χ_{lf} and SIRM in the uppermost zone (Z-I: 3.5 to 8.5 mbsf) indicate decline in magnetic mineral content (Fig. 2a,b). The Z-II (13.0 to 32.81 mbsf), Z-III (34.29 to 98.71 mbsf), and Z-V (99.62 to 124.83 mbsf) are marked by a notable enhancement in χ_{lf} and SIRM, but exhibit different trends in ARM/IRM_{2.5T} profile (Fig. 2a-c). The Z-IV (133.87 to 143.19 mbsf) is marked by relatively lower χ_{lf} and SIRM compared to Z-III and Z-V. A trend of rise in magnetic grain size proxy (ARM/IRM_{2.5T}) in Z-IV and Z-V suggest the presence of fine-grained magnetic particles (Fig. 2c; Peters & Dekkers, 2003). A gradual downcore rise in ARM/IRM_{2.5T} in Z-II (8.5 to 18.29 mbsf), Z-III (43.4 to 72.53 mbsf), and Z-V (122.9 to 143.19 mbsf) suggest the dominance of fine-grained authigenic magnetite or greigite (Fig. 2c; Rodelli et al., 2019; Lin et al., 2021).

S-ratio is a magnetic mineralogy diagnostic proxy and provides information on the relative proportion of ferri- and antiferromagnetic particles in the sediment sample (Liu et al., 2012). Overall, the S-ratio profile show uniformity and close to unity, but exhibit a distinct shift between Z-I and other zones (Fig. 2e). This observation suggest that bulk magnetic mineralogy of Z-II to Z-V is unequivocally characterized by ferrimagnetic minerals. Comparatively, Z-I is dominated by the presence of hard coercive minerals as seen through a drop in S-ratio (Fig. 2e). Magnetic iron sulfide diagnostic proxy ($SIRM/\chi_{lf}$; Larrasoaña et al., 2007) mimics the S-ratio profile and showed a marked shift at the end of Z-I suggesting the significant increase in proportion of ferrimagnetic (greigite, pyrrhotite) iron sulfides (Fig. 2e; Snowball & Thompson, 1990; Maher & Thompson, 1999; Peters & Dekkers, 2003). In general, TOC and $CaCO_3$ content showed large fluctuations throughout the core (Fig. 2f, g). Initially, TOC decreases from 3.5 mbsf to 18.19 mbsf in Z-I and later increases downcore from 24.2 mbsf to 94.63 mbsf except in Z-IV (Fig. 2f). The $CaCO_3$ profile showed peak in Z-II and does not exhibit any specific trends in other zones (Fig. 2g).

4.2. Temperature-dependent magnetic susceptibility (χ -T) Curves and Day Plot

The χ -T data has been utilized for determining the changes in magnetic mineral composition of marine sediments (Liu et al., 2005). The χ -T curves for selected bulk sediment samples representing different magnetic zones are shown in Fig. 3a-n. A major decline in magnetization between 419°C and 644°C in majority of the samples imply that the bulk magnetic mineralogy is governed by titanomagnetite (Fig. 3; Dunlop et al., 1997). A minor rise in χ between 270°C and 492°C suggest the dominance of either titanomagnetite particles possessing wide range of Ti-contents (Lattard et al., 2006), or conversion of pyrite into magnetite due to heating (Fig. 3; Passier et al., 2001). The day plot shows that all the samples lie on the SD-MD mixing line (Day et al., 1977; Dunlop, 2002) (Fig. 4d).

4.3. Mineralogical analyses of magnetic particles and optical microscopy

SEM-EDS analyses complement our rock magnetic observations and further confirmed that titanomagnetite is the major magnetic mineral in the studied core (Figs. 5-10 and Figs. S1-S6). Based on the composition and morphology, we identified detrital ferrimagnetic (titanomagnetite), altered (titanomaghemite, titanohematite) and diagenetically formed iron sulfide (pyrite) grains of various sizes and shapes in the different sediment magnetic zones (Figs. 5-10 and Figs. S1-S6). Detrital titanomagnetite grains in the uppermost zone (Z-I) appears fresh and well-preserved (Fig. 5, S1). Signatures of diagenetic dissolution and low-temperature maghemitization of detrital titanomagnetite particles including etching, pits, skeleton lamellae, and distinct shrinkage cracks are noticed (Figs. 7-

8). Few titanohematite particles showed lamellae-like features reflecting pervasive oxidation of primary titanomagnetite (Fig. 8b-c). Diagenetically formed pyrite occur as individual crystals on the surface of Fe-Ti grains (Figs. 6-10) in the methanic zones (Z-II to Z-V). Several bands of diagenetically formed pyrite nodules of various size and shape were found to occur throughout the core (Fig. 11).

5. Discussion

Room and high-temperature based magnetic data combined with SEM-EDS observations provided valuable insights on the magnetic mineral assemblages in core NGHP-01-20A. Data showed that the magnetic particles have encountered severe diagenetic dissolution, maghemitization and sulphidization in the sulfidic and methanic zones. Rock magnetic record of core NGHP-01-20A helped to define five sediment magnetic zones. Here, we evaluate the magnetic mineral composition, grain size, and morphology based information to systematically examine how magnetic particles respond to primary (detrital) and secondary (diagenesis, authigenesis) processes in a marine gas hydrate bearing sedimentary system of the K-G basin, Bay of Bengal.

5.1. Rock magnetism of Sediment Core NGHP-01-20A

Rock magnetism of core NGHP-01-20A representing deep-seated gas hydrate system is carried by complicated magnetic mineral assemblages comprised of detrital (titanomagnetite, silicate-hosted magnetic inclusions), altered (titanomaghemite, titanohematite), diagenetic (pyrite), and authigenic (magnetite, greigite) as confirmed through rock magnetic, SEM-EDS and optical microscopy (Figs. 2,3, 5-10,12). Microbial iron-reduction in anoxic sediments is driven by (a) dissimilatory iron-reducing bacteria (DIRB) (Moskowitz, 1995; Roberts, 2015), (b) methanogens which favour methanogenesis to iron-reduction (Sivan et al., 2016), and (3) iron-reduction coupled to AOM (Egger et al., 2014). Magnetic grain size diagnostic ($ARM/IRM_{2.5T}$) proxy has been successfully used to detect the presence of fine-grained authigenic magnetite (Fig. 2c; Dillon & Bleil, 2006; Lin et al., 2021) in methanic sediments. A recent study by Lin et al (2021) reported a novel authigenic nanoscale magnetite source in methane seep sediments from South China Sea. They attributed the increase in ARM/SIRM in methanic zone to the presence of authigenic magnetite formed as a result of microbial iron-reduction process which permitted the newly formed magnetite to survive the sulfidic dissolution and favoured preservation. Initial decrease of $ARM/IRM_{2.5T}$ values in core NGHP-01-20A could be linked with the preferential dissolution of fine-grained magnetic particles in the upper most sulfidic zone (Z-I). Downcore increase of $ARM/IRM_{2.5T}$ in Z-II (vicinity of present-day SMTZ) and methanic zones (Z-III: 43.4 to 72.53 mbsf, Z-IV: 98.71 to 102.8 mbsf;

Z-V: 133.87 to 143.19 mbsf) can be attributed to the magnetite authigenesis linked with microbial iron-reduction process which might have permitted the preservation of newly formed authigenic magnetite (Fig. 2c; Dillon & Bleil, 2006; Roberts, 2015; Chang et al., 2016; Rodelli et al., 2019; Gaikwad et al., 2021; Lin et al., 2021). As highlighted by Lin et al., 2021, χ_{lf} fluctuations in methanic zones (Z-III to Z-V) indicate vertical migration of SMTZ in core NGHP-01-20A controlled by varying methane fluxes (Fig. 2h), which is common in gas hydrate bearing sites for example in continental margin offshore of Argentina and Uruguay (Riedinger et al., 2005), southwestern Taiwan (Horng & Chen, 2006), and Nankai Margin, southwestern Japan (Kars & Kodama, 2015a; Shi et al., 2017). It is highly likely that, higher sulfide concentration produced during intense AOM driven by enhanced methane seepage events in the past might have promoted pyrite formation at paleo-SMTZ intervals in Z-III to Z-V. During low methane seepage, downward diffusing sea water sulfate might have enhanced the oxidation of previously formed iron sulfides at paleo-SMTZ position resulting in the production of secondary iron (oxyhydr)oxides which acted as a potential reactive iron source for magnetite authigenesis (Lin et al., 2021). We therefore propose that the authigenic formation of fine-grained magnetite in the anoxic (methanic) environment of Z-II (8.5 to 18.29 mbsf), Z-III (43.4 to 72.53 mbsf), Z-IV (98.71 to 118.2 mbsf), and Z-V (122.9 to 143.19 mbsf) of core NGHP-01-20A is most likely driven by magnetite authigenesis coupled microbial iron-reduction processes. Biogenic (magnetite, greigite) minerals formed by biomineralization are widespread in marine sediments (Karlin & Levi, 1983; Mann et al., 1990; Moskowitz et al., 1993; Tarduno & Wilkison, 1996; Chang et al., 2013, 2014; Roberts, 2015; Rodelli et al., 2019). As confirmed through SEM-EDS, the magnetic particles are mainly dominated by detrital titanomagnetites. The presence of biogenic minerals is expected, but we did not detect any signature in the analyzed samples probably due to the limitation of our detection (microscopy, rock magnetic) techniques. However, TEM and FORC may provide confirmation on its presence.

Magnetic iron sulfide diagnostic proxy ($SIRM/\chi_{lf}$) revealed two distinct trends (Fig. 2d; Snowball & Thompson, 1990; Maher & Thompson, 1999; Peters & Dekkers, 2003). Initial lower values of $SIRM/\chi_{lf}$ values in Z-I suggest the presence of coarse-grained magnetic particles (Fig. 2d). Relatively higher values and consistent trend of $SIRM/\chi_{lf}$ from Z-II to Z-V points on the plausible presence of fine-grained authigenic greigite in these zones (Fig. 2d; Larrasoana et al., 2007; Kars et al., 2015; Amiel et al., 2020). The dominance of greigite in these zones suggest that the in situ geochemical conditions probably supported the authigenic formation of greigite by inhibiting the pyritization process in the past. High sedimentation interval generated by intense monsoon-driven weathering and erosional processes might have resulted in a weaker and short-lived AOM which

produced low concentration of dissolved hydrogen sulphide and preferentially affected the completion of pyritization process and rather favoured the greigite formation (Fig. 2d; Housen & Musgrave, 1996; Larrasoña et al., 2007; Kars & Kodama, 2015; Dewangan et al., 2013; Badesab et al., 2019). Lack of presence of greigite in our SEM-EDS records can be explained based on the fact that previously formed unstable ferrimagnetic greigite might have got transformed into more stable pyrite (Kao et al., 2004; Larrasoña et al. 2007; Kars & Kodama, 2015). The presence of pyrite (Figs. 6, 7, 10) within magnetically enhanced intervals (Z-II, Z-III, Z-V) provide support for the above interpretation. The overall contribution of paramagnetic (pyrite) minerals transformed from ferrimagnetic (greigite) mineral phase is negligible, compared to the bulk magnetic signal exhibited by Fe-Ti particles of varying size and concentration. Hence, the bulk magnetic susceptibility values in this core remained high even after the significant conversion of ferrimagnetic (greigite) to paramagnetic (pyrite) iron sulfide.

5.2. Lines of evidence of diagenetic dissolution, maghemitization and oxidation of titanomagnetite in a rapidly deposited methane-bearing sediments from the Bay of Bengal.

Precise identification of magnetic minerals in methanic sediments is a prerequisite to constrain the information related to primary (provenance) and post-depositional (diagenetic/authigenic) processes from the magnetic proxies. In the present study, SEM-EDS observations (Figs. 5-10, S1-S6) on magnetic particles from sulfidic and methanic sedimentary zones yielded direct evidence to help understand the impact of detrital sedimentation, diagenetic and authigenic processes on the rock magnetism of a sediment core NGHP-01-20A. SEM observations combined with EDS analyses provided information on the overall composition, grains size, morphology, state of preservation and genesis of sedimentary (detrital and diagenetic) magnetic minerals (Figs. 5-10, S1-S6). Based on the comprehensive documentation, we successfully identified six different types of magnetic mineral assemblages (Figs. 5-10, S1-S6). Detrital titanomagnetite, with angular, irregular, spherical and well-defined octahedral with micron and submicron sized particles mainly related to DVP constitute the type-1 particles (Fig. 5a,b, Fig. 6a-d, Fig. 7b, Fig. 9a,b, Fig. 10a-c). Titanomaghemites represent type – 2 particles and are characterized by shrinkage cracks formed as a result of low temperature maghemitization process after initial deposition (Fig. 7c,e, Fig. 8a, Fig. 10a). Titanohematites exhibiting lamellae like feature resulting from oxidation of titanomagnetite represent type-3 particles (Fig. 7a,c, d, Fig. 8b,c, Fig. 10b). Diagenetically altered titanomagnetites constitute type-4 particles and showed dissolution features including severe etching, pits, and skeleton lamellar like structures (Fig. 6a,d, Fig. 7a,d, Fig. 10b). Fine-grained diagenetically formed iron sulfides (pyrite,) occurring on Fe-Ti grains represent type – 5 particles (Fig. 5a, Fig. 6c,

Fig. 7,c,d, Fig. 10a). Silicate hosted magnetic grains formed from exsolution within host silicates constitute type – 6 assemblage (Fig. 12). The optical microscopy showed pyrite nodules exhibiting partial, intermediate and full oxidation stages of magnetic particles (Fig. 11).

5.2.1. Detrital Sedimentation

The Deccan basalts of DVP are the principal source for the continental slope sediment off K-G basin (Sangode et al., 2001; Dewangan et al., 2013; Usapkar et al., 2014). Dominance of well-preserved coarse-grained (Figs. 5-10) titanomagnetite grains throughout the core suggest that the detrital magnetic particles are mainly sourced from Deccan basalts and were delivered to the Bay of Bengal by the Krishna and Godavari river systems. Detrital titanomagnetites grains from all sediment magnetic zones showed high variability in shape, size, composition and state of alteration and preservation (Figs. 5-10 and Fig. S1-S6). Majority of the particles are well-preserved and idiomorphic in shape. In general, titanomagnetite grains throughout the core exhibited well-preserved structure as well as skeleton and ilmenite-lamellae which is mainly evolved by the low-temperature exsolution of titanomagnetite (Figs. 5-10; Garming et al., 2007; Dillon & Franke, 2009; Nowaczyk, 2011). Few magnetic grains showed numerous shrinkage cracks and lamellar structure which provided evidence for maghemitization of Fe-Ti particles (Figs. 7,8,10; Özdemir & Dunlop, 2010; Chang et al., 2013; Roberts, 2015; Qian et al., 2021). In Z-III, we noticed that titanomagnetite particles showed clear etching on the surface indicative action of etching acids which created wooden bark-like texture (Fig. 7-8). The titanomagnetite and titanomaghemite grains are characterized by shrinkage cracks and skeleton lamellae wherein lattice in the crystals have been disturbed due to diagenetic dissolution and low-temperature exsolution from the titanomagnetite which probably led to the creation of such structures in the titanomagnetite grains (Garming et al., 2005, 2007; Nowaczyk, 2011; Just et al., 2012; Gaikwad et al., 2021).

5.2.2. Diagenetic dissolution and maghemitization of Fe-Ti particles

Diagenetic dissolution of titanomagnetite and preservation of titanohematite is characteristic of a strongly reducing environment (Garming et al., 2007; Canfield & Thamdrup, 2009; Roberts, 2015). The oxidized individual magnetic grains showed moderate to high degree of dissolution of the low Ti-bearing titanomagnetite particles thereby leaving the high Ti-rich titanohematite lamellae intact. Such magnetic particles were commonly noticed in Z-II and Z-III (Figs. 6-8). Previously Garming et al. (2005) highlighted that preferential diffusion of Fe²⁺ out of titanomagnetite grains during diagenesis is much easier compared to hematite and titanohematite particles which are highly stable and exhibit strong resistance against dissolution. Presence of abundant titanohematite grains in

the same magnetic zones (Z-II and Z-III) provide evidence on the stability of the Ti-rich magnetic particles which offered more resistance to diagenetic dissolutions compared to titanomagnetite (Hounslow et al., 1995; Poulton et al., 2004; Garming et al., 2005; Franke et al., 2007; Nowaczyk, 2011; Roberts, 2015 João et al., 2021).

In marine sediments, partial magnetite oxidation (maghemitization) is common process and can significantly influence the room as well as temperature-dependent rockmagnetic parameters (Karlin, 1990; Özdemir & Dunlop, 2010; Yamazaki & Solheid, 2011; Roberts, 2015). Maghemitization processs mainly involves preferential leaching of Fe^{2+} out of titanomagnetite, since it gets quickly detached from the mineral structure as compared to Fe^{3+} and create lattice vacancies (Cornell & Schwertmann, 1996; Smirnov & Tarduno, 2000; Garming et al., 2005; Roberts, 2015). Irregular, curved shrinkage cracks on the surface of magnetic particles resulting from the internal stress caused by surficial oxidation are the characteristics of maghemitization (Fig. 7-8; Petersen & Vali, 1987; Nowaczyk, 2011; Höfken et al., 2021). A recent rock magnetic and electron microscopy based studies on the magnetic particles from eastern Mediterranean sediments (Qian et al., 2021) and ridge flank sediments of the East Pacific Rise (Höfken et al., 2021) provided useful insights into the step-wise maghemitization process wherein the surfaces of magnetite particles gets maghemitized at oxidation fronts. The SEM-EDS data of core NGHP-01-20A provided evidence for the dominance of maghemitization process as indicated by the irregular surface cracks and fragmentation on the titanomagnetite particles especially in Z-II and Z-III (Figs. 7-8). Similar signatures of minor low-temperature oxidation were also noticed in Z-II (Fig. 6a,d) and Z-V (Fig. 10a). These observations suggest that maghemitization was a significant process in both sulfidic (Z-I) and methanic (Z-II to Z-V) environments.

5.2.3. Sulphidization

Diagenetically formed pyrite (yellowish-dark brown-orange) nodules were noticed in all sediment magnetic zones except Z-IV (Fig. 11). Few pyrite nodules revealed thick layering and showed strong affinity to the magnet during the separation process (Fig. 11). Past studies reported similar growth of pyrite rim over the ferrimagnetic (magnetite and greigite) core for example, in Dead Sea basin (Ebert et al., 2018), South Island, New Zealand (Roberts & Turner 1993; Rowan & Roberts, 2006), and K-G basin, Bay of Bengal (Badesab et al., 2020a). As highlighted by Larrasoña et al. (2007), the pyrite growth over magnetic particles in the studied core (NGHP-01-20A) is indicative of the diagenetic transformation wherein dissolved sulfide most likely interacted with highly reactive iron available on the surface of ferrimagnetic iron bearing oxide minerals and proceeded further towards pyritization. Moreover, Ebert et al (2018) explained that during

sulphidization, the reactive iron is selectively leached out from the residual titanomagnetites and gets directly transformed into the pyrite layer which grow over the magnetite core. In the analyzed samples, the growth of pyrite over the magnetite core (Fig. 11) suggest that the reactive iron required for pyritization was most likely made available through the surficial leaching of iron from abundant Fe-Ti particles. Non-uniform (yellowish-dark brown-orange colored) layering on the magnetite grains reveals the signature of different stages of pyritization of magnetic particles (Fig. 11). Our interpretation is consistent with the observations of Rowan & Roberts (2006), Rowan et al (2009), and Ebert et al (2018) which reported similar growth of iron sulfide i.e., pyrite rim over the titanomagnetite grains and further highlighted that the magnetism exhibited by the titanomagnetite core is strong and would therefore show affinity towards magnetic probes as noticed during separation of magnetic particles.

Preservation of organic carbon in a rapidly depositing marine sediments is controlled by the sedimentation rates, composition of organic matter, oxygen availability, sediment texture, temperature, and rates of oxic and suboxic processes (Burdige, 2007; Galy et al., 2007; Zonneveld et al., 2010). A good covariation between increased χ_{lf} and TOC content in magnetically enhanced zones (Z-II, Z-III, Z-V) of core NGHP-01-20A is noticed (Fig. 2a,f). Rigorous sediment mixing and reworking in rapidly depositing marine sedimentary system can significantly affect the oxidation of labile organic matter and enhance its preservation (Joao et al., 2021). Elevated TOC content in magnetite-rich zones (Z-II, Z-III, Z-V) can be reconciled with the efficient preservation of labile organic matter due to increased sediment deposition. Higher TOC content (Fig. 2a,f) in Z-II, Z-III and Z-V could also be attributed to the changes in the burial and degradation of organic matter due to non-steady sedimentation which might have affected the remineralization rate and consequently constrained the methane-induced diagenetic reactions (Rey et al., 2005; Joao et al., 2021). Fluctuation in χ_{lf} SIRM, and TOC content within these zones (Z-II, Z-III, Z-V) indicate continuous shifting of the diagenetic fronts at this site (Fig. 2a,b,f). Such phenomena is well-reported from a rapidly depositing sediments from continental margins offshore of Argentina and Uruguay (Riedinger et al., 2005), offshore of North Island, New Zealand (Rowan & Roberts, 2006), K-G basin, Bay of Bengal (Joao et al., 2021; Mazumdar et al., 2012), and Nankai Margin, southwestern Japan (Kars & Kodama, 2015b). Methane-derived authigenic carbonates (MDAC) are distributed throughout the core NGHP-01-20A and is indicative of paleo-SMTZ positions. The mineralogy of MDAC comprised of iron-rich carbonate and low-magnesium calcite (LMC) (Teichert et al., 2014). The LMC is present in sediment magnetic zones exhibiting low χ_{lf} (Z-I: 9.6 mbsf, Z-III: 33.1 mbsf, Z-IV: 121.5 mbsf, 124.8 mbsf) (Fig. 2a) and depleted $\delta^{13}C$ (-27.45 to -15.26 ‰ VPDB; Teichert et

al., 2014) values suggesting a major role of AOM in these magnetically altered sediment intervals. Concurrently, the presence of siderite especially in magnetic enhanced zones (Z-III: 106.5 mbsf and Z-V: 133.6 mbsf, Teichert et al., 2014) suggest that formation of enriched carbonates are mainly linked with silicate weathering reactions coupled to microbial methanogenesis which did not altered χ_f (Solomon et al., 2014; Torres et al., 2020).

5.2.4. Silicate-hosted magnetic mineral inclusion

Magnetic mineral inclusions within silicate grains are ubiquitously distributed in marine sediments, and their size varies between few nanometers to several micrometres with different morphologies (Hounslow, 1996; Hounslow & Morton, 2004; Roberts, 2015; Chang et al., 2016; 2021). The occurrence of titanomagnetite as well as diagenetically formed iron sulfides (greigite) nanoparticles as inclusions within silicate minerals were reported from hemipelagic marine sediments offshore, Japan (Chang et al., 2016), Okhotsk Sea (Jiang et al., 2021), North Pacific Ocean (Hong et al., 2019), and gas hydrate bearing sediments from the Bay of Bengal (Badesab et al., 2020; Gaikwad et al., 2021). Recent study focussing on magnetic mineral diagenesis in methanic sediments from the Bay of Bengal proposed that silicate weathering and silica diagenesis triggered by past methane seepage events played a crucial role in the preservation of greigite as inclusions within silicate matrix (Badesab et al., 2020a). Optical microscopy analyses on the separated quartz grains (+ 63 micron.m) of core NGHP-01-20A revealed the presence of nanometre-sized magnetic particles hosted within silicates in addition to fine magnetic crystals occurring as surface coating (Fig. 12; Nowaczyk, 2011; Ebert et al., 2018). We suggest that the silicate-hosted magnetic inclusions protected the ferrimagnetic (titanomagnetite, magnetite, greigite) particles within silicate matrix against the surrounding diagenetic fronts through geologic times and prevented its further conversion. However, TEM-EDS analyses on the quartz grains is further warranted to confirm the mineralogy of the fine-grained magnetic particles occurring as inclusions within silicate grains and can be taken up as a dedicated independent study in future.

5.3. Control of rapid sedimentation events on the rock magnetism (*detrital vs diagenetic processes*)

Occurrence of high sedimentation rate events in the K-G basin is well-recorded from seismic and multibeam bathymetry data, age and sediment physical property data (Ramana et al., 2007; Ramprasad et al., 2011; Yamamoto et al., 2018). Large detrital magnetite grains with variable Ti-contents were found to be highly concentrated in a few magnetically enhanced sediment zones (Z-II, Z-III, Z-V) (Figs. 2a, 6,7,8,10). The presence of fine-grained SD magnetite can be attributed to the

authigenic magnetite formation via microbial iron-reduction as reflected in downcore rise in ARM/IRM_{2.5T} (Fig. 2c; Rodelli et al., 2019; Lin et al., 2021), or from smectite-derived iron during progressive diagenetic illitization (McCabe et al., 1989; Kars et al., 2021). The electron microscopy in combination with EDS analyses on the magnetic extracts confirmed the presence of abundant unaltered coarser magnetic grains primarily of detrital origin in each zone (Figs. 5-10, Figs. S1 – S6). This observation suggest that the higher sedimentation rates facilitated the rapid burial and preservation of the detrital magnetic particles soon after deposition which resulted in the formation of three distinct magnetite-rich bands in Z-II, Z-III and Z-V (Fig. 2). Few magnetic particles close to SMTZ depth showed the presence of partly dissolved titanomagnetite (Fig. 6), suggesting the partial dissolution of the detrital titanomagnetite particles close to the SMTZ. It is most likely that, a significant portion of the detrital ferromagnetic particles survived the reductive diagenetic dissolution at SMTZ predominantly due to the increased sedimentation rate (Riedinger et al., 2005, 2014; Egger et al., 2017; Badesab et al., 2019; Johnson et al., 2021; Joao et al., 2021) or due to elevated episodic pulses of rising methane in Z-II to Z-V that led to quick migration of SMTZ fronts (Fig. 2h; Sivan et al., 2007). Abundant occurrence of titanomagnetite coupled with high χ_{lf} in the deeper part (Z-V; Fig. 2a, 10) of the core NGHP-01-20A also suggest that rapid sedimentation events favored the preservation of magnetic particles and inhibited the pyritization reactions by altering the AOM process which caused decline in the production of sufficient hydrogen sulfide concentration required to trigger intense diagenesis.

6. Conclusions

In this study, we systematically investigated a sediment core from the Bay of Bengal by combining bulk rock magnetic analyses and SEM-EDS observations to unravel the effect of range of diagenetic processes on the magnetic minerals in the sulfidic and methanic sediments. The electron microscope results are consistent with the bulk magnetic properties. Our work demonstrates that a focussed approach based on SEM-EDS analyses of magnetic particles from sulfidic and methanic zones provided valuable insights into the mineralogy, genesis and their state of preservation and also enhances the interpretative value of rock magnetic proxies. We summarized our findings in a conceptual diagenetic model for Site NGHP-01-20 which clearly explains the selective response of magnetic minerals to varying stages of diagenesis (reductive dissolution, maghemitization, sulphidization) which is constrained by the combined influence of methane-induced geochemical processes and high sedimentation rates in the marine gas hydrate system (Fig. 13).

6. Acknowledgement

Authors are grateful to Director, CSIR-National Institute of Oceanography (NIO), for his support, and permission to publish this work. We thank the Directors of NIOT, NCAOR, advisor MOES, NGHP (India) for supporting this study. The NGHP coordinated by DGH is thanked for providing sediment samples of Indian National Gas Hydrate Expedition 01 for this study. Special thanks to Shri. T. Ramprasad for providing support in accessing NGHP sediment core samples. We also thank the Director, CSIR-National Geophysical Research Institute, Hyderabad for allowing us to conduct specialized rock magnetic measurements. Thanks to Areef Sardar and Dr. Mandar Nanajkar for providing assistance with SEM-EDS analysis and optical microscopy. We greatly acknowledge the constructive comments from the editor and two anonymous reviewers who helped to improve this manuscript considerably. The data used in this study has been archived at CSIR-NIO data repository and the link to access data online (<https://publication-data.nio.org/s/iK8qL58PzZLLRT9>). The work was performed under CSIR project MSEEPS, MLP-2015. The authors declare no conflict of interests. This is CSIR-NIO publication no. XXXX.

Data Availability Statement

The data used in this study has been archived at CSIR-NIO data repository and the link to access data online (<https://publication-data.nio.org/s/iK8qL58PzZLLRT9>).

Figure Captions:

Fig. 1: Sediment core locations map of NGHP-01-20A (present study), NGHP-01-10D, MD161/Stn-8, NGHP-01-03B, NGHP-01-05C, NGHP-01-14A, NGHP-01-15A, NGHP-01-16A and NGHP-01-07B, in the Krishna-Godavari (K-G) basin, Bay of Bengal. Bathymetry data of the studied area was obtained from GEBCO Compilation Group665 (2020) GEBCO 2020 Grid (10.5285/a29c5465-b138-234d-e053-6c86abc040b9).

Fig. 2: Depth variations of (a–e) selected magnetic and (f–h) geochemical parameters for sediment core NGHP-01-20A. Three magnetite-rich bands exhibiting higher values of magnetic susceptibility have been identified. Magnetite-rich band in sediment magnetic zones Z– II, Z-III and Z-V are highlighted by pink, green and yellow color shading respectively. The depth of sulfate-methane transition zone (SMTZ) is marked by blue arrow. The sediment depth intervals of pyrite nodules occurrence are highlighted in solid black arrows (horizontal). (Please note that χ_{lf} = low frequency magnetic susceptibility; ARM = anhysteretic remanent magnetization; and SIRM = saturation isothermal remanent magnetization).

Fig. 3 (a–n): Temperature dependence of magnetic susceptibility (χ -T) for selected representative samples from the five sediment zones (Z-I, Z-II, Z-III, Z-IV, Z-V) of the studied sediment core NGHP-01-20A are presented. Solid red and blue lines indicate heating and cooling curves respectively. The respective magnetic minerals titanomagnetite (TM) and pyrite (Py) identified based on the χ -T curves are mentioned in the plot.

Fig. 4 (a–f): Bivariate scatter plots of magnetic parameters: magnetic susceptibility (χ_{lf}), saturation isothermal remanent magnetization (SIRM), ARM/IRM_{2.5T}, SIRM/ χ_{lf} , total organic carbon (TOC), calcium carbonate (CaCO₃) and Day plot of NGHP-01-20A from the Krishna-Godavari (K-G) basin, Bay of Bengal. The gray arrows are used only to highlight the observed trends in plots.

Fig. 5 (a–b): Scanning electron microscopy (SEM) images of magnetic particles extracted from sediment magnetic zone (Z-I) of the sediment core NGHP-01-20A. (a-b) well-preserved detrital titanomagnetite (TM) grain. The blue color square represent the area selected for generation of energy dispersive X-ray spectra (EDS).

Fig. 6 (a–d): Scanning electron microscopy (SEM) images of magnetic particles extracted from sediment magnetic zone (Z-II) of the sediment core NGHP-01-20A. (a,d) Diagenetically altered titanomagnetite (TM) grains exhibiting dissolution features. Signatures of minor low-temperature oxidation are noticed, (b) Detrital titanomagnetite (TM) grain showing partial dissolution, and (c) Diagenetically formed iron-sulfides (pyrite; Py) occur as individual fine-grained crystals on the surface of titanomagnetite (TM) grain. The blue color square represent the area selected for generation of energy dispersive X-ray spectra (EDS).

Fig. 7 (a–f): Scanning electron microscopy (SEM) images of magnetic particles extracted from sediment magnetic zone (Z-III) of the sediment core NGHP-01-20A. (a,d,f) Titanohematite (TH) grains exhibiting skeletal and lamellae like structure resulting from oxidation of titanomagnetite, (b) Well-preserved detrital titanomagnetite (TM) grains, (c,e) Titanomaghemite (TMG) grains exhibiting shrinkage cracks typical features linked with low-temperature maghemitization. The blue color square represent the area selected for generation of energy dispersive X-ray spectra (EDS).

Fig. 8 (a–c): Scanning electron microscopy (SEM) images of magnetic particles extracted from sediment magnetic zone (Z-III) of the sediment core NGHP-01-20A (a) Titanomaghemite (TMG)

grain characterized by shrinkage cracks formed due to low-temperature maghemitization, (b,c) Titanohematite (TH) grains exhibiting lamellae-like features reflecting pervasive oxidation of titanomagnetite. The blue color square represent the area selected for generation of energy dispersive X-ray spectra (EDS).

Fig. 9 (a–b): Scanning electron microscopy (SEM) images of magnetic particles extracted from sediment magnetic zone (Z-IV) of the sediment core NGHP-01-20A. (a,b) Well-preserved detrital titanomagnetite (TM) grains. The blue color square represent the area selected for generation of energy dispersive X-ray spectra (EDS).

Fig. 10 (a–c): Scanning electron microscopy (SEM) images of magnetic particles extracted from sediment magnetic zone (Z-V) of the sediment core NGHP-01-20A. (a,b) Titanomagnetite (TM) grains of detrital origin. Few grains showed signature of low-temperature maghemitization, (b) Titanohematite (TH) grains exhibiting lamellae-like features resulting from oxidation of titanomagnetite, (c) Well-preserved detrital titanomagnetite (TM) grains. The blue color square represent the area selected for generation of energy dispersive X-ray spectra (EDS).

Fig. 11 (a – d): Optical microscopic images of the pyrite nodules separated from the sediment core NGHP-01-20A. The overgrowth (orange-reddish color) of pyrite on the magnetite grains is highlighted using arrows (white color).

Fig. 12 (a–d): Optical microscopic images of the representative coarse fractions ($>63 \mu\text{m}$) from the different magnetic zones of sediment core NGHP-01-20A are presented. Fine-grained magnetic inclusion within host silicate minerals ($>63 \mu\text{m}$) fractions are marked (see red arrows).

Fig. 13: Conceptual model explaining the constraints of detrital, diagenetic, authigenic, maghemitization and sulphidization processes on the evolution of magnetic mineralogies at Site NGHP-01-20. The arrows (red color) on the magnetic susceptibility profile of core NGHP-01-20A represent the carbonate occurrence depths.

Supplementary Fig. S1 (a–b): Energy dispersive spectroscopy (EDS) data of respective scanning electron microscopy (SEM) images of the sediment magnetic zone (Z-I) presented in Fig. 5.

Supplementary Fig. S2 (a–d): Energy dispersive spectroscopy (EDS) data of respective scanning electron microscopy (SEM) images of the sediment magnetic (Z-II) presented in Fig. 6.

Supplementary Fig. S3 (a–f): Energy dispersive spectroscopy (EDS) data of respective scanning electron microscopy (SEM) images of the sediment magnetic zone (Z-III) presented in Fig. 7.

Supplementary Fig. S4 (a–c): Energy dispersive spectroscopy (EDS) data of respective scanning electron microscopy (SEM) images of the sediment magnetic zone (Z-III) presented in Fig. 8.

Supplementary Fig. S5 (a–b): Energy dispersive spectroscopy (EDS) data of respective scanning electron microscopy (SEM) images of the sediment magnetic zone (Z-V) presented in Fig. 9.

Supplementary Fig. S6 (a–c): Energy dispersive spectroscopy (EDS) data of respective scanning electron microscopy (SEM) images of the sediment magnetic zone (Z-V) presented in Fig. 10.

Supplementary Fig. S7: Comparison of volume-specific shipboard multi-sensore core logger (MSCL) magnetic susceptibility (2006) to the laboratory based mass-normalized magnetic susceptibility (χ) of core NGHP-01-20A.

References

Abubakar, R., Muxworthy, A. R., Sephton, M. A., Southern, P., Watson, J. S., Fraser, A. J., and Almeida, T. P. (2015). Formation of magnetic minerals at hydrocarbon-generation conditions. *Marine and Petroleum Geology*, 68, 509-519. <https://doi.org/10.1016/j.marpetgeo.2015.10.003>

Amiel, N., Shaar, R., and Sivan, O. (2020). The Effect of Early Diagenesis in Methanic Sediments on Sedimentary Magnetic Properties: Case Study From the SE Mediterranean Continental Shelf. *Frontiers in Earth Science*, 8:283. <https://doi.org/10.3389/feart.2020.00283>

Anitha, G., Ramana, M. V., Ramprasad, T., Dewangan, P., and Anuradha, M. (2014). Shallow geological environment of Krishna–Godavari offshore, eastern continental margin of India as inferred from the interpretation of high resolution sparker data. *Journal of Earth System Science*, 123(2), 329-342. <https://doi.org/10.1007/s12040-013-0399-3>

Ao, H., Deng, C., Dekkers, M. J., and Liu, Q. (2010). Magnetic mineral dissolution in Pleistocene fluvio-lacustrine sediments, Nihewan Basin (North China). *Earth and Planetary Science Letters*, 292(1-2), 191-200. <https://doi.org/10.1016/j.epsl.2010.01.035>

Aubourg, C., and Pozzi, J. P. (2010). Toward a new < 250 C pyrrhotite–magnetite geothermometer for claystones. *Earth and Planetary Science Letters*, 294(1-2), 47-57. <https://doi.org/10.1016/j.epsl.2010.02.045>

Badesab F, Dewangan P, Gaikwad V, Kars M, Kocherla M, Krishna KS, Sangode SJ, Deenadayalan K, Kumar P, Naikgaonkar O, and Ismaiel M. (2019). Magnetic mineralogical approach for the exploration of gas hydrates in the Bay of Bengal. *Journal of Geophysical Research: Solid Earth*. <https://doi.org/10.1029/2019JB01746>

Badesab, F., Dewangan, P., and Gaikwad, V. (2020c). Magnetic mineral diagenesis in a newly discovered active cold seep site in the Bay of Bengal. *Front. Earth Sci.* <https://doi.org/10.3389/feart.2020.592557>

Badesab, F., Dewangan, P., Gaikwad, V., Sebastian, J. G., and Venkateshwarlu, M. (2020b). A rock magnetic perspective of gas hydrate occurrences in a high-energy depositional system in the Krishna-Godavari basin, Bay of Bengal. *Geo-Mar. Lett.*, 1-15. <https://doi.org/10.1007/s00367-020-00646-8>

Badesab, F., Dewangan, P., Usapkar, A., Kocherla, M., Peketi, A., Mohite, K., Sangode, S.J., Deenadayalan, K. (2017). Controls on evolution of gas-hydrate system in the Krishna-Godavari basin, offshore India. *Geochem Geophys*, 18(1), 52–74. <https://doi.org/10.1002/2016GC006606>

Badesab, F., Gaikwad, V., and Dewangan, P. (2020a). Controls on greigite preservation in a gas hydrate system of the Krishna-Godavari basin, Bay of Bengal. *Geo-Mar. Lett.*, 40(4), 439-452. <https://doi.org/10.1007/s00367-019-00604-z>

Bastia, R. (2007). Geological setting and petroleum systems of India's east coast offshore basins: concepts and applications. Technology, Publications, Dehradun, India, 204, Eastern Book, Delhi, India.

- Berner, R. A. (1984). Sedimentary pyrite formation: An update. *Geochimica et Cosmochimica Acta*, 48(4), 605–615. [https://doi.org/10.1016/0016-7037\(84\)90089-9](https://doi.org/10.1016/0016-7037(84)90089-9)
- Biksham, G., and Subramanian, V. (1988). Sediment transport of the Godavari River basin and its controlling factors. *J. Hydrol.*, 101(1-4), 275-290. [https://doi.org/10.1016/0022-1694\(88\)90040-6](https://doi.org/10.1016/0022-1694(88)90040-6)
- Bloemendal, J., King, J.W., Hall, F.R., and Doh, S.J. (1992) Rock magnetism of late Neogene and Pleistocene deep-sea sediments: relationship to sediment source, diagenetic processes, and sediment lithology. *J. Geophys. Res. Solid Earth*, 96:4361–4375. <https://doi.org/10.1029/91JB03068>
- Borowski, W. S., Paull, C. K., and Ussler, W. III (1996). Marine pore-water sulfate profiles indicate in situ methane flux from underlying gas hydrate. *Geology*, 24(7), 655–658. [https://doi.org/10.1130/0091-7613\(1996\)024<0655:MPWSPI>2.3.CO;2](https://doi.org/10.1130/0091-7613(1996)024<0655:MPWSPI>2.3.CO;2)
- Burdige DJ (2007) Preservation of organic matter in marine sediments: controls, mechanisms, and an imbalance in sediment organic carbon budgets? *Chem Rev.* 2007 Feb; 107(2):467-85. <https://10.1021/cr050347q>
- Canfield, D. E. (1989). Reactive iron in marine sediments. *Geochimica et cosmochimica acta*, 53(3), 619-632. [https://doi.org/10.1016/0016-7037\(89\)90005-7](https://doi.org/10.1016/0016-7037(89)90005-7)
- Canfield, D. E., and Berner, R. A. (1987). Dissolution and pyritization of magnetite in anoxic marine sediments. *Geochimica et Cosmochimica Acta*, 51(3), 645–659. [https://doi.org/10.1016/0016-7037\(87\)90076-7](https://doi.org/10.1016/0016-7037(87)90076-7)
- Canfield, D. E., and Thamdrup, B. O. (2009). Towards a consistent classification scheme for geochemical environments, or, why we wish the term ‘suboxic’ would go away. *Geobiology* 7, 385–392. <https://doi.org/10.1111/j.1472-4669.2009.00214.x>
- Chang, L., Heslop, D., Roberts, A. P., Rey, D., and Mohamed, K. J. (2016). Discrimination of biogenic and detrital magnetite through a double Verwey transition temperature. *Journal of Geophysical Research: Solid Earth*, 121(1), 3-14. <https://doi.org/10.1002/2015JB012485>
- Chang, L., Hong, H., Bai, F., Wang, S., Pei, Z., Paterson, G. A., Heslop, D., Roberts, A.P., Huang, B., Tauxe, L. and Muxworthy, A.R. (2021). Detrital remanent magnetization of single-crystal silicates with magnetic inclusions: constraints from deposition experiments. *Geophysical Journal International*, 224(3), 2001-2015. <https://doi.org/10.1093/gji/ggaa559>
- Chang, L., Vasiliev, I., van Baak, C., Krijgsman, W., Dekkers, M.J., Roberts, A.P., Gerald, J.D.F., van Hoesel, A. and Winklhofer, M. (2014). Identification and environmental interpretation of diagenetic and biogenic greigite in sediments: A lesson from the Messinian Black Sea. *Geochemistry, Geophysics, Geosystems*, 15(9), pp.3612-3627. <https://doi.org/10.1002/2014GC005411>
- Chang, L., Winklhofer, M., Roberts, A. P., Heslop, D., Florindo, F., Dekkers, M. J., et al. (2013). Low-temperature magnetic properties of pelagic carbonates: Oxidation of biogenic magnetite and identification of magnetosome chains. *J. Geophys. Res. Solid Earth*, 118(12), 6049-6065. <https://doi.org/10.1002/2013JB010381>
- Channell, J. E. T., and Stoner, J. S. (2002). Plio-Pleistocene magnetic polarity stratigraphies and diagenetic magnetite dissolution at ODP Leg 177 Sites (1089, 1091, 1093 and 1094). *Marine Micropaleontology*, 45(3-4), 269-290. [https://doi.org/10.1016/S0377-8398\(02\)00032-4](https://doi.org/10.1016/S0377-8398(02)00032-4)

Choudhuri, M., Guha, D., Dutta, A., Sinha, S., and Sinha, N. (2010). Spatio-temporal variations and kinematics of shale mobility in the Krishna-Godavari basin, India. In: AAPG Hedberg Conference, Port of Spain, Port of Spain, Trinidad and Tobago, 5–7 June 2006.

Collett, T., Riedel, M., Cochran, J. R., Boswell, R., Presley, J., Kumar, P., et al. (2008). Indian National Gas Hydrate Program, Expedition - 01, Initial report, Directorate General of Hydrocarbons, Ministry of Petroleum and Natural gas, India.

Cornell, R.M., Schwertmann, U. (1996). The Iron Oxides: Structure, Properties, Reactions, Occurrences, and Uses. VCH Publishers, New York (753 pp.).

Das, A., and Krishnaswami, S. (2007). Elemental geochemistry of river sediments from the Deccan Traps, India: implications to sources of elements and their mobility during basalt–water interaction. *Chemical Geology*, 242(1-2), 232-254. <https://doi.org/10.1016/j.chemgeo.2007.03.023>

Day, R., Fuller, M., Schmidt, V.A. (1977). Hysteresis properties of titanomagnetites: grain-size and compositional dependence. *Phys Earth Planet Inter* 13(4):260–267. [https://doi.org/10.1016/0031-9201\(77\)90108-X](https://doi.org/10.1016/0031-9201(77)90108-X)

Dewangan, P., Basavaiah N., Badesab F. K., Usapkar A., Mazumdar A., Joshi R., and Ramprasad T. (2013). Diagenesis of magnetic minerals in a gas hydrate/cold seep environment off the Krishna–Godavari basin, Bay of Bengal, *Marine Geology*, 340, 57–70, <https://doi.org/10.1016/j.margeo.2013.04.016>

Dewangan, P., Ramprasad, T., Ramana, M. V., Mazumdar, A., Desa, M., and Badasab, F. (2008). Shale Tectonics in the Continental Slope and Rise Regions of Krishna-Godavari Basin, Bay of Bengal: Implication in Gas-Hydrate Exploration. In AGU Fall Meeting Abstracts (Vol. 2008, pp. OS33A-1313).

Dewangan, P., Ramprasad, T., Ramana, M. V., Mazumdar, A., Desa, M., and Badesab, F. K. (2010). Seabed morphology and gas venting features in the continental slope region of Krishna-Godavari basin, Bay of Bengal: Implications in gas-hydrate exploration. *Mar. Petrol. Geol.*, 27(7), 1628–1641. <https://doi.org/10.1016/j.marpetgeo.2010.03.015>

Dewangan, P., Sriram G., Ramprasad T., Ramana M. V., and Jaiswal P. (2011). Fault system and thermal regime in the vicinity of site NGHP-01-10, Krishna–Godavari basin, Bay of Bengal. *Marine and Petroleum Geology*, 28, 1899–1914, <https://doi:10.1016/j.marpetgeo.2011.03.009>.

Dewangan, P., Sriram, G., Kumar, A., Mazumdar, A., Peketi, A., Mahale, V. et al. (2021). Widespread occurrence of methane seeps in deep-water regions of Krishna-Godavari basin, Bay of Bengal. *Mar. Petrol. Geol.*, 104783. <https://doi.org/1016/j.marpetgeo.2020.104783>

Dillon, M., and Bleil, U. (2006). Rock magnetic signatures in diagenetically altered sediments from the Niger deep-sea fan. *Journal of Geophysical Research: Solid Earth*, 111(B3). <https://doi.org/10.1029/2004JB003540>

Dillon, M., and Franke, C. (2009). Diagenetic alteration of natural Fe–Ti oxides identified by energy dispersive spectroscopy and low-temperature magnetic remanence and hysteresis measurements. *Physics of the Earth and Planetary Interiors*, 172(3-4), 141-156. <https://doi.org/10.1016/j.pepi.2008.08.003>

Dunlop, D. J., Özdemir, Ö., and Schmidt, P. W. (1997). Paleomagnetism and paleothermometry of the Sydney Basin 2. Origin of anomalously high unblocking temperatures. *Journal of Geophysical Research*, 102(B12), 27, 285–27,295. <https://doi.org/10.1029/97JB02478>

Dunlop, D.J. (2002). Theory and application of the Day plot (Mrs/Ms versus Hcr/Hc) 1. Theoretical curves and tests using titanomagnetite data. *J. Geophys. Res.* 107, B2056. <http://dx.doi.org/10.1029/2001JB000486>.

Ebert, Y., Shaar, R., Emmanuel, S., Nowaczyk, N., and Stein, M. (2018). Overwriting of sedimentary magnetism by bacterially mediated mineral alteration. *Geology*, 46(4), 291-294. <https://doi.org/10.1130/G39706.1>

Egger, M., Hagens, M., Sapart, C. J., Dijkstra, N., van Helmond, N. A., Mogollón, J. M., Risgaard-Petersen, N., van der Veen, C., Kasten, S., Riedinger, N. and Böttcher, M.E., Thomas, R., Bo, B. J., Caroline, P.S. (2017). Iron oxide reduction in methane-rich deep Baltic Sea sediments. *Geochimica et Cosmochimica Acta*, 207, 256-276. <https://doi.org/10.1016/j.gca.2017.03.019>

Elmore, R. D., Kelley, J., Evans, M., and Lewchuk, M. T. (2001). Remagnetization and orogenic fluids: testing the hypothesis in the central Appalachians. *Geophysical Journal International*, 144(3), 568-576. <https://doi.org/10.1046/j.0956-540X.2000.01349.x>

Esteban, L., Enkin, R. J., and Hamilton, T. (2008). Gas hydrates and magnetism: Comparative geological settings for diagenetic analysis. In ICGH. Proceedings of the 6th International Conference on Gas Hydrates (pp. 1-9).

Franke, C., von Dobeneck, T., Drury, M. R., Meeldijk, J. D., and Dekkers, M. J. (2007). Magnetic petrology of equatorial Atlantic sediments: Electron microscopy results and their implications for environmental magnetic interpretation. *Paleoceanography*, 22(4). <https://doi.org/10.1029/2007PA001442>

Gaikwad, V. V., Badesab, F. K., Dewangan, P., Kotha, M. (2021). Diagenesis of Magnetic Minerals in Active/Relict Methane Seep: Constraints from Rock Magnetism and Mineralogical Records from Bay of Bengal. *Front. Earth Sci.* 9, 60. <https://doi.org/10.3389/feart.2021.638594>

Galy, V., France-Lanord, C., Beyssac, O. et al. Efficient organic carbon burial in the Bengal fan sustained by the Himalayan erosional system. *Nature* 450, 407–410 (2007). <https://doi.org/10.1038/nature06273>

Garming, J. F. L., Bleil, U., and Riedinger, N. (2005). Alteration of magnetic mineralogy at the sulfate–methane transition: Analysis of sediments from the Argentine continental slope. *Physics of the Earth and Planetary Interiors*, 151(3-4), 290–308. <https://doi.org/10.1016/j.pepi.2005.04.001>

Garming, J. F. L., Von Dobeneck, T., Franke, C., and Bleil, U. (2007). Low-temperature partial magnetic self-reversal in marine sediments by magnetostatic interaction of titanomagnetite and titanohematite intergrowths. *Geophysical Journal International*, 170(3), 1067-1075. <https://doi.org/10.1111/j.1365-246X.2007.03504.x>

Höfken, A. F., Dobeneck, T. V., Kuhn, T., and Kasten, S. (2021). Impact of upward oxygen diffusion from the oceanic crust on the magnetostratigraphy and iron biomineralization of East Pacific ridge-flank sediments. *Frontiers in Earth Science*. <https://doi.org/10.3389/feart.2021.689931>

- Hong, H., Chang, L., Hayashida, A., Roberts, A.P., Heslop, D., Paterson, G.A., Kodama, K. and Tauxe, L. (2019). Paleomagnetic recording efficiency of sedimentary magnetic mineral inclusions: implications for relative paleointensity determinations. *Journal of Geophysical Research: Solid Earth*, 124(7), pp.6267-6279. <https://doi.org/10.1029/2018JB016859>
- Hong, W. L., Solomon, E. A., and Torres, M. E. (2014). A kinetic-model approach to quantify the effect of mass transport deposits on pore water profiles in the Krishna–Godavari Basin, Bay of Bengal. *Marine and petroleum geology*, 58, 223-232. <https://doi.org/10.1016/j.marpetgeo.2014.06.014>
- Hong, C. S. (2018). Unusual magnetic properties of sedimentary pyrrhotite in methane seepage sediments: Comparison with metamorphic pyrrhotite and sedimentary greigite. *J. Geophys. Res. Solid Earth*, 123(6), 4601-4617. <https://doi.org/10.1002/2017JB015262>
- Hong, C. S., and Kuo-Hang, C. (2006). Complicated magnetic mineral assemblages in marine sediments offshore of southwestern Taiwan: possible influence of methane flux on the early diagenetic process. *TAO: Terrestrial, Atmospheric and Oceanic Sciences*, 17(4), 1009.
- Hounslow, M. W., and Morton, A. C. (2004). Evaluation of sediment provenance using magnetic mineral inclusions in clastic silicates: comparison with heavy mineral analysis. *Sedimentary Geology*, 171(1-4), 13-36. <https://doi.org/10.1016/j.sedgeo.2004.05.008>
- Hounslow, M.W. (1996). Ferrimagnetic Cr and Mn spinels in sediments: residual magnetic minerals after diagenetic dissolution. *Geophys. Res. Lett.* 23, 2823–2826. <https://doi.org/10.1029/96GL01327>
- Hounslow, M.W., Maher, B.A., Thistlewood, L. (1995). Magnetic mineralogy of sandstones from the Lunde Formation (late Triassic), northern North Sea, UK: origin of the palaeomagnetic signal. *Geol. Soc. Lond. Spec. Publ.* 98, 119–147. <https://doi.org/10.1144/GSL.SP.1995.098.01.07>
- Housen, B. A., and Musgrave, R. J. (1996). Rock-magnetic signature of gas hydrates in accretionary prism sediments. *Earth Planet. Sci. Lett.*, 139(3-4), 509–519. [https://doi.org/10.1016/0012-821X\(95\)00245-8](https://doi.org/10.1016/0012-821X(95)00245-8)
- Jiang, X.D., Zhao, X.Y., Zhao, X., Jiang, Z.X., Chou, Y.M., Zhang, T.W., Yang, X.Q. and Liu, Q.S. (2021). Quantifying Contributions of Magnetic Inclusions Within Silicates to Marine Sediments: A Dissolution Approach to Isolating Volcanic Signals for Improved Paleoenvironmental Reconstruction. *Journal of Geophysical Research: Solid Earth*, 126(10), p.e2021JB022680. <https://doi.org/10.1029/2021JB022680>
- João, H. M., Badesab, F., Gaikwad, V., Kocherla, M., Deenadayalan, K. (2021). Controls of mass transport deposit and magnetic mineral diagenesis on the sediment magnetic record from the Bay of Bengal. *Mar. Petrol. Geol.* 128, 104994. <https://doi.org/10.1016/j.marpetgeo.2021.104994>
- Johnson, J. E., Phillips, S. C., Clyde, W. C., Giosan, L., and Torres, M. E. (2021). Isolating Detrital and Diagenetic Signals in Magnetic Susceptibility Records From Methane-Bearing Marine Sediments. *Geochemistry, Geophysics, Geosystems*, 22(9), e2021GC009867. <https://doi.org/10.1029/2021GC009867>
- Johnson, J. E., Phillips, S. C., Torres, M. E., Piñero, E., Rose, K. K., and Giosan, L. (2014). Influence of total organic carbon deposition on the inventory of gas hydrate in the Indian continental margins. *Marine and Petroleum Geology*, 58, 406-424. <https://doi.org/10.1016/j.marpetgeo.2014.08.021>

- Jørgensen, B. B., Böttcher, M. E., Lüschen, H., Neretin, L. N., and Volkov, I. I. (2004). Anaerobic methane oxidation and a deep H₂S sink generate isotopically heavy sulfides in Black Sea sediments. *Geochim. Cosmochim. Acta*, 68(9), 2095–2118. <https://doi.org/10.1016/j.gca.2003.07.017>
- Just, J., Heslop, D., von Dobeneck, T., Bickert, T., Dekkers, M.J., Frederichs, T., Meyer, I., Zabel, M., (2012). Multiproxy characterization and budgeting of terrigenous end-members at the NW African continental margin. *Geochem., Geophys., Geosys.*, 13(9). <https://doi.org/10.1029/2012GC004148>
- Kao, S. J., Horng, C. S., Roberts, A. P., and Liu, K. K. (2004). Carbon–sulfur–iron relationships in sedimentary rocks from southwestern Taiwan: Influence of geochemical environment on greigite and pyrrhotite formation. *Chemical Geology*, 203(1-2), 153–168. <https://doi.org/10.1016/j.chemgeo.2003.09.007>
- Karlin, R. (1990). Magnetite diagenesis in marine sediments from the Oregon continental margin. *Journal of Geophysical Research: Solid Earth*, 95(B4), 4405-4419. <https://doi.org/10.1029/JB095iB04p04405>
- Karlin, R., and Levi, S. (1983). Diagenesis of magnetic minerals in recent haemipelagic sediments. *Nature*, 303(5915), 327. <https://doi.org/10.1038/303327a0>
- Kars, M. M., and Kodma K. (2015a), Authigenesis of magnetic minerals in gas hydrate bearing sediments in the Nankai Trough, Offshore Japan, *Geochemistry, Geophysics, Geosystems*, 16, 947–961, <https://doi.org/10.1002/2014GC005614>.
- Kars, M., and Kodama, K. (2015b). Rock magnetic characterization of ferrimagnetic iron sulfides in gas hydrate-bearing marine sediments at Site C0008, Nankai Trough, Pacific Ocean, off-coast Japan. *Earth, Planets and Space*, 67(1), 118. <https://doi.org/10.1186/s40623-015-0287-y>
- Kars, M., Aubourg, C., Labaume, P., Berquó, T.S., Cavailhes, T. (2014). Burial diagenesis of magnetic minerals: new insights from the Grès D'Annot transect (SE France). *Minerals* 4, 667–689. <https://doi.org/10.3390/min4030667>
- Kars, M., Aubourg, C., Pozzi, J.P., Janots, D. (2012). Continuous production of nanosized magnetite through low grade burial. *Geochem. Geophys. Geosyst.* 13, Q08Z48. <http://dx.doi.org/10.1029/2012GC004104>.
- Kars, M., Greve, A., Zerbst, L., (2021). Authigenic greigite as an indicator of methane diffusion in gas hydrate-bearing sediments of the Hikurangi Margin, New Zealand. *Front. Earth Sci.* 9, 80. <https://doi.org/10.3389/feart.2021.603363>
- Kars, M., Musgrave, R. J., Hoshino, T., Jonas, A. S., Bauersachs, T., Inagaki, F., Kodama, K., (2018). Magnetic mineral diagenesis in a high temperature and deep methanic zone in Izu rear arc marine sediments, northwest Pacific Ocean. *J. Geophys. Res. Solid Earth*. 123(10), 8331-8348. <https://doi.org/10.1029/2018JB015861>
- Kasten, S., Zabel, M., Heuer, V., and Hensen, C. (2003). Processes and signals of nonsteady-state diagenesis in deep-sea sediments and their pore waters. In *The South Atlantic in the Late Quaternary*, (pp. 431–459). Berlin, Heidelberg: Springer. <https://doi.org/10.1016/j.gca.2007.08.019>
- Katz, B., Elmore, R. D., Cogoini, M., Engel, M. H., and Ferry, S. (2000). Associations between burial diagenesis of smectite, chemical remagnetization, and magnetite authigenesis in the Vocontian

trough, SE France. *Journal of Geophysical Research: Solid Earth*, 105(B1), 851-868. <https://doi.org/10.1029/1999JB900309>

Kawamura, N., Oda, H., Ikehara, K., Yamazaki, T., Shioi, K., Taga, S., Hatakeyama, S., Torii, M. (2007). Diagenetic effect on magnetic properties of marine core sediments from the southern Okhotsk Sea. *Earth Planets Space* 59, 83–93. <https://doi.org/10.1186/BF03352680>

Kim, J., Dong, H., Yang, K., Park, H., Elliott, W.C., Spivack, A., Koo, T.H., Kim, G., Morono, Y., Henkel, S. and Inagaki, F. (2019). Naturally occurring, microbially induced smectite-to-illite reaction. *Geology*, 47(6), pp.535-539. <https://doi.org/10.1130/G46122.1>

Knittel, K., and Boetius, A. (2009). Anaerobic oxidation of methane: progress with an unknown process. *Annual review of microbiology*, 63, 311-334. <https://doi.org/10.1146/annurev.micro.61.080706.093130>

Köster, M., Kars, M., Schubotz, F., Tsang, M.Y., Maisch, M., Kappler, A., Morono, Y., Inagaki, F., Heuer, V.B., Kasten, S. and Henkel, S. (2021). Evolution of (Bio-) Geochemical Processes and Diagenetic Alteration of Sediments Along the Tectonic Migration of Ocean Floor in the Shikoku Basin off Japan. *Geochemistry, Geophysics, Geosystems*, 22(8), p.e2020GC009585. <https://doi.org/10.1029/2020GC009585>

Kumar, P., Collett, T. S., Boswell, R., Cochran, J. R., Lall, M., Mazumdar, A., et al. (2014). Geologic implications of gas hydrates in the offshore of India: Krishna-Godavari Basin, Mahanadi Basin, Andaman Sea, Kerala–Konkan Basin. *Mar. Petrol. Geol.*, 58,29–98. <https://doi.org/10.1016/j.marpetgeo.2014.07.031>

Larrasoña, J. C., Roberts, A. P., Musgrave, R. J., Gràcia, E., Piñero, E., Vega, M., et al. (2007). Diagenetic formation of greigite and pyrrhotite in gas hydrate marine sedimentary systems. *Earth Planet. Sci. Lett.*, 261(3-4), 350–366. <https://doi.org/10.1016/j.epsl.2007.06.032>

Lin, Z., Sun, X., Roberts, A.P., Strauss, H., Lu, Y., Yang, X., et al. (2021). A novel authigenic magnetite source for sedimentary magnetization. *Geology*. 49(4), 360-365. <https://doi.org/10.1130/G48069.1>

Liu, Q., Deng, C., Yu, Y., Torrent, J., Jackson, M. J., Banerjee, S. K., and Zhu, R. (2005). Temperature dependence of magnetic susceptibility in an argon environment: implications for pedogenesis of Chinese loess/palaeosols. *Geophysical Journal International*, 161(1), 102-112. <https://doi.org/10.1111/j.1365-246X.2005.02564.x>

Liu, Q., Roberts, A. P., Larrasoña Larrasoana, J. C., Banerjee, S. K., Guyodo, Y., Tauxe, L., and Oldfield, F. (2012). Environmental magnetism: principles and applications. *Reviews of Geophysics*, 50(4). <https://doi.org/10.1029/2012RG000393>

Maher, B. A., and Thompson, R. (Eds.). (1999). *Quaternary climates, environments and magnetism*. Cambridge University Press.

Mann, S., Sparks, N. H., Frankel, R. B., Bazylinski, D. A., and Jannasch, H. W. (1990). Biomineralization of ferrimagnetic greigite (Fe₃S₄) and iron pyrite (FeS₂) in a magnetotactic bacterium. *Nature*, 343(6255), 258-261. <https://doi.org/10.1038/343258a0>

- Mazumdar A., Dewangan P., Peketi A., Gullapalli S., Kalpana M. S., Naik G. P., et al. (2019). The first record of active methane (cold) seep ecosystem associated with shallow methane hydrate from the Indian EEZ. *J. of Earth Sys. Sci.*, 128:18, <https://doi.org/10.1007/s12040-018-1044-y>
- Mazumdar, A., Joao, H.M., Peketi, A., Dewangan, P., Kocherla, M., Joshi, R.K., Ramprasad, T. (2012). Geochemical and geological constraints on the composition of marine sediment pore fluid: possible link to gas hydrate deposits. *Mar. Petrol. Geol.* 38 (1), 35–52. <https://doi.org/10.1016/j.marpetgeo.2012.07.004>
- Mazumdar, A., Kocherla, M., Carvalho, M.A., Peketi, A., Joshi, R.K., Mahalaxmi, P. (2015). Geochemical characterization of the Krishna-Godavari and Mahanadi offshore basin (Bay of Bengal) sediments: a comparative study of provenance. *Mar. Petrol. Geol.*, 60, 18-33. <https://doi.org/10.1016/j.marpetgeo.2014.09.005>
- McCabe, C., Jackson, M., Saffer, B. (1989). Regional patterns of magnetite authigenesis in the Appalachian Basin: implications for the mechanism of late Paleozoic remagnetization. *J. Geophys. Res.* 94, 10,429–10,443.
- Moskowitz, B. M., Frankel, R. B., and Bazylinski, D. A. (1993). Rock magnetic criteria for the detection of biogenic magnetite. *Earth and Planetary Science Letters*, 120(3-4), 283-300. [https://doi.org/10.1016/0012-821X\(93\)90245-5](https://doi.org/10.1016/0012-821X(93)90245-5)
- Musgrave, R. J., Kars, M., and Vega, M. E. (2019). Progressive and Punctuated Magnetic Mineral Diagenesis: The Rock Magnetic Record of Multiple Fluid Inputs and Progressive Pyritization in a Volcano-Bounded Basin, IODP Site U1437, Izu Rear Arc. *J. Geophys. Res. Solid Earth*, 124(6), 5357-5378. <https://doi.org/10.1029/2018JB017277>
- Neretin, L. N., Böttcher, M. E., Jørgensen, B. B., Volkov, I. I., Lüschen, H., and Hilgenfeldt, K. (2004). Pyritization processes and greigite formation in the advancing sulfidization front in the upper Pleistocene sediments of the Black Sea 1. *Geochim. Cosmochim. Acta*, 68(9), 2081–2093. [https://doi.org/10.1016/S0016-7037\(03\)00450-2](https://doi.org/10.1016/S0016-7037(03)00450-2)
- Novosel, I., G. D. Spence, and R. D. Hyndman (2005), Reduced magnetization produced by increased methane flux at a gas hydrate vent, *Mar. Geol.*, 216(4), 265–274. <https://doi.org/10.1016/j.margeo.2005.02.027>.
- Nowaczyk, N. R. (2011). Dissolution of titanomagnetite and sulphidization in sediments from Lake Kinneret, Israel. *Geophys. J. Inter.*, 187(1), 34-44. <https://doi.org/10.1111/j.1365-246X.2011.05120.x>
- Özdemir, Ö., and Dunlop, D.J. (2010). Hallmarks of maghemitization in low-temperature remanence cycling of partially oxidized magnetite nanoparticles. *J. Geophys. Res.* 115, B02101. <http://dx.doi.org/10.1029/2009JB006756>.
- Panieri, G., Graves, C. A., and James, R. H. (2016). Paleo-methane emissions recorded in foraminifera near the landward limit of the gas hydrate stability zone offshore western Svalbard. *Geochem., Geophys., Geosys.*, 17, 521–537. <https://doi.org/10.1002/2015GC006153>
- Passier, H.F., de Lange, G.J., Dekkers, M.J. (2001). Magnetic properties and geochemistry of the active oxidation front and the youngest sapropel in the eastern Mediterranean Sea. *Geophys. J. Int.* 145, 604–614. <https://doi.org/10.1046/j.0956-540x.2001.01394.x>

- Peters, C., and Dekkers, M. J. (2003). Selected room temperature magnetic parameters as a function of mineralogy, concentration and grain size. *Phys. Chem. Earth, Parts A/B/C*, 28(16-19), 659-667. [https://doi.org/10.1016/S1474-7065\(03\)00120-7](https://doi.org/10.1016/S1474-7065(03)00120-7)
- Petersen, N., and Vali, H. (1987). Observation of shrinkage cracks in ocean floor titanomagnetites. *Phys. Earth Planet. Inter.* 46, 197–205.
- Petersen, N., T. Von Dobeneck, andamp; H. Vali (1986). Fossil bacterial magnetite in deep-sea sediments from the South Atlantic Ocean, *Nature*, 320, 611–615. <https://doi.org/10.1038/320611a0>
- Phillips, S. C., Johnson, J. E., Underwood, M. B., Guo, J., Giosan, L., and Rose, K. (2014). Long-timescale variation in bulk and clay mineral composition of Indian continental margin sediments in the Bay of Bengal, Arabian Sea, and Andaman Sea. *Marine and Petroleum Geology*, 58, 117-138. <https://doi.org/10.1016/j.marpetgeo.2014.06.018>
- Poulton, S. W., Krom, M. D., and Raiswell, R. (2004). A revised scheme for the reactivity of iron (oxyhydr) oxide minerals towards dissolved sulfide. *Geochimica et cosmochimica acta*, 68(18), 3703-3715. <https://doi.org/10.1016/j.gca.2004.03.012>
- Prabhakar, K. N., and Zutshi, P. L. (1993). Evolution of southern part of Indian East Coast basin. *Journal of Geological Society of India*, 41, 215–230.
- Qian, Y., Heslop, D., Roberts, A. P., Hu, P., Zhao, X., Liu, Y., et al. (2021). Low-temperature magnetic properties of marine sediments—Quantifying magnetofossils, superparamagnetism, and maghemitization: Eastern Mediterranean examples. *Journal of Geophysical Research: Solid Earth*, 126, e2021JB021793. <https://doi.org/10.1029/2021JB021793>
- Raiswell, R., Canfield, D.E. (2012). The iron biogeochemical cycle past and present. *Geochem. Perspect.* 1, 1–215.
- Ramana, M. V., Ramprasad, T., Kamesh Raju, K. A., and Desa, M. (2007). Occurrence of gas hydrates along the continental margins of India, particularly the Krishna-Godavari off shore basin. *International Journal of Environmental Studies*, 64(6), 675–693. <https://doi.org/10.1080/00207230701476321>
- Ramana, M. V., Ramprasad, T., Paropkari, A. L., Borole, D. V., Rao, B. R., Karisiddaiah, S. M., and Gonsalves, M. J. (2009). Multidisciplinary investigations exploring indicators of gas hydrate occurrence in the Krishna–Godavari Basin offshore, east coast of India. *Geo-Marine Letters*, 29(1), 25–38. <https://doi.org/10.1007/s00367-008-0121-7>
- Ramesh R., and V. Subramanian (1988), Temporal, spatial and size variation in the sediment transport in the Krishna River basin, India, *Journal of Hydrology*, 98, 53–65. [https://doi.org/10.1016/0022-1694\(88\)90205-3](https://doi.org/10.1016/0022-1694(88)90205-3)
- Ramprasad, T., Dewangan, P., Ramana, M. V., Mazumdar, A., Karisiddaiah, S. M., Ramya, E. R., andSriram, G. (2011). Evidence of slumping/sliding in Krishna–Godavari offshore basin due to gas/fluid movements. *Marine and Petroleum Geology*, 28(10), 1806–1816. <https://doi.org/10.1016/j.marpetgeo.2011.02.007Rao 2001>
- Rao, G. N. (2001). Sedimentation, stratigraphy, and petroleum potential of Krishna-Godavari basin, East Coast of India. *AAPG Bulletin.*, 85(9), 1623–1643.

- Rao, V. P. (1991). Clay mineral distribution in the continental shelf sediments from Krishna to Ganges river mouth, east coast of India. *Ind. J. Mar. Sci.*, 20, 7–12.
- Reidinger, N., Pfeifer, K., Kasten, S., Garhing, J. F. L., Vogt, C., and Hensen C. (2005). Diagenetic alteration of magnetic signals by anaerobic oxidation of methane related to a change in sedimentation rate, *Geochim. Cosmochim. Acta*, 69, 4117–4126, <https://doi.org/10.1016/j.gca.2005.02.004>.
- Reilly, B. T., McCormick, M. L., Brachfeld, S. A., Haley, B. A. (2020). Authigenic ferromagnetic iron sulfide preservation due to non- steady state diagenesis: A perspective from Perseverance Drift, North western Weddell Sea. *Geochem., Geophys., Geosys.* e2020GC009380. <https://doi.org/10.1029/2020GC009380>
- Riedinger, N., Formolo, M. J., Lyons, T. W., Henkel, S., Beck, A., Kasten, S. (2014). An inorganic geochemical argument for coupled anaerobic oxidation of methane and iron reduction in marine sediments. *Geobiology* 12(2), 172-181. <https://doi.org/10.1111/gbi.12077>
- Roberts, A. P. (2015). Magnetic mineral diagenesis. *Earth-Sci. Rev.*, 151, 1–47. <https://doi.org/10.1016/j.earscirev.2015.09.010>
- Roberts, A. P., and Turner, G. M. (1993). Diagenetic formation of ferrimagnetic iron sulphide minerals in rapidly deposited marine sediments, South Island, New Zealand. *Earth and Planetary Science Letters*, 115(1-4), 257-273. [https://doi.org/10.1016/0012-821X\(93\)90226-Y](https://doi.org/10.1016/0012-821X(93)90226-Y)
- Roberts, A. P., and Weaver, R. (2005). Multiple mechanisms of remagnetization involving sedimentary greigite (Fe₃S₄). *Earth Planet. Sci. Lett.*, 231, 263–277. <https://doi.org/10.1016/j.epsl.2004.11.024>
- Roberts, A.P., Reynolds, R.L., Verosub, K.L., Adam, D.P. (1996). Environmental magnetic implications of greigite (Fe₃S₄) formation in a 3 million year lake sediment record from Butte Valley, Northern California. *Geophys. Res. Lett.* 23, 2859–2862.
- Rodelli, D., Jovane, L., Giorgioni, M., Rego, E. S., Cornaggia, F., Benites, M., et al., (2019). Diagenetic fate of biogenic soft and hard magnetite in chemically stratified sedimentary environments of Mamanguá Ría, Brazil. *J. Geophys. Res. Solid Earth.* 124 (3), 2313–2330. <https://doi.org/10.1029/2018JB016576>
- Rodelli, D., Jovane, L., Roberts, A. P., Cypriano, J., Abreu, F., Lins, U. (2018). Fingerprints of partial oxidation of biogenic magnetite from cultivated and natural marine magnetotactic bacteria using synchrotron radiation. *1226 Environ. Microbiol. Rep.* 10 (3), 337–343. <https://doi.org/10.1111/1758-2229.12644>
- Rowan, C. J., and Roberts, A. P. (2006). Magnetite dissolution, diachronous greigite formation, and secondary magnetizations from pyrite oxidation: Unravelling complex magnetizations in Neogene marine sediments from New Zealand. *Earth Planet. Sci. Lett.*, 241(1-2), 119–137. <https://doi.org/10.1016/j.epsl.2005.10.017>
- Rowan, C. J., Roberts, A. P., and Broadbent, T. (2009). Reductive diagenesis, magnetite dissolution, greigite growth and paleomagnetic smoothing in marine sediments: A new view. *Earth Planet. Sci. Lett.*, 277(1-2), 223–235. <https://doi.org/10.1016/j.epsl.2008.10.016>

- Sahu, H.S., Raab, M.J., Kohn, B.P., Gleadow, A.J.W. (2013). Thermal history of the Krishna-Godavari basin, India: Constraints from apatite fission track thermochronology and organic maturity data. *Journal of Asian Earth Sciences*, 73, 1-20.
- Sangode, S. J., R. Sinha, B. Phartiyal, O. S. Chauhan, R. K. Mazari, T. N. Bagati, N. Suresh, S. Mishra, R. Kumar, and P. Bhattacharjee (2007), Environmental magnetic studies on some quaternary sediments of varied depositional settings in the Indian sub-continent, *Quat. Int.*, 159, 102–118, <https://doi.org/10.1016/j.quaint.2006.08.015>.
- Sangode, S. J., Suresh, N., and Bagati, T. N. (2001). Godavari source in the Bengal fan sediments: Results from magnetic susceptibility dispersal pattern. *Curr. Sci.*, 80 (5), 660–664.
- Shankar, U., and Riedel, M. (2010). Seismic and heat flow constraints from the gas hydrate system in the Krishna-Godavari basin, India. *Mar. Geol.*, 276(1–4), 1–13. <https://doi.org/10.1016/j.margeo.2010.06.006>
- Shanmugam, G., Shrivastava, S. K., and Das, B. (2009). Sandy debrites and tidalites of Pliocene reservoir sands in upper slope canyon environments, offshore Krishna–Godavari Basin (India): implications. *Journal of Sedimentary Research*, 79(9), 736–756. <https://doi.org/10.2110/jsr.2009.076>
- Shi, M., Wu, H., Roberts, A.P., Zhang, S., Zhao, X., Li, H., Su, X., Yang, T., Chang, L., Hu, P., and Zhao, X. (2017). Tectonic, climatic, and diagenetic control of magnetic properties of sediments from Kumano Basin, Nankai margin, southwestern Japan. *Marine Geology*, 391, pp.1-12. <https://doi.org/10.1016/j.margeo.2017.07.006>
- Sivan, O., Schrag, D. P., and Murray, R. W. (2007). Rates of methanogenesis and methanotrophy in deep-sea sediments. *Geobiology* 5, 141–151. <https://doi.org/10.1111/j.1472-4669.2007.00098.x>
- Smirnov, A.V., and Tarduno, J.A. (2000). Low-temperature magnetic properties of pelagic sediments (Ocean Drilling Program Site 805C): tracers of maghemitization and magnetic mineral reduction. *J. Geophys. Res.* 105, 16,457–16,471.
- Snowball, I., and Thompson, R. (1990). A stable chemical remanence in Holocene sediments. *J. Geophys. Res. Solid Earth*, 95(B4), 4471-4479. <https://doi.org/10.1029/JB095iB04p04471>
- Solomon, E. A., Spivack, A. J., Kastner, M., Torres, M. E., and Robertson, G. (2014). Gas hydrate distribution and carbon sequestration through coupled microbial methanogenesis and silicate weathering in the Krishna–Godavari Basin, offshore India. *Marine and Petroleum Geology*, 58, 233-253. <https://doi.org/10.1016/j.marpetgeo.2014.08.020>
- Tarduno, J.A., and Wilkison, S. (1996). Non-steady state magnetic mineral reduction, chemical lock-in, and delayed remanence acquisition in pelagic sediments. *Earth Planet. Sci. Lett.* 144, 315–326.
- Teichert, B. M. A., Johnson, J. E., Solomon, E. A., Giosan, L., Rose, K., Kocherla, M., ... and Torres, M. E. (2014). Composition and origin of authigenic carbonates in the Krishna–Godavari and Mahanadi Basins, eastern continental margin of India. *Marine and Petroleum Geology*, 58, 438-460. <https://doi.org/10.1016/j.marpetgeo.2014.08.023>
- Treude, T., Knittel, K., Blumenberg, M., Seifert, R., and Boetius, A. (2005). Subsurface microbial methanotrophic mats in the Black Sea. *Applied and Environmental Microbiology*, 71(10), 6375-6378. <https://doi.org/10.1128/AEM.71.10.6375-6378.2005>

Usapkar, A., Dewangan, P., Kocherla, M., Ramprasad, T., Mazumdar, A., and Ramana, M. V. (2014). Enhanced methane flux event and sediment dispersal pattern in the Krishna–Godavari offshore basin: Evidences from rock magnetic techniques. *Mar. Petrol. Geol.*, 58, 461–475 <https://doi.org/10.1016/j.marpetgeo.2014.08.008>

Yamamoto, Y., Chiyonobu, S., Kanamatsu, T., Ahagon, N., Aoike, K., Kamiya, N., and Kinoshita, M. (2018). Repeated large-scale mass transport deposits and consequent rapid sedimentation in the western part of the Bay of Bengal, India. *Geological Society, London, Special Publications*. In G. London: Geological Society (Vol. 477SP477–12). <https://doi.org/10.1144/SP477.12>

Yamazaki, T., and Solheid, P. (2011). Maghemite-to-magnetite reduction across the Fe-redox boundary in a sediment core from the Ontong-Java Plateau: influence on relative palaeointensity estimation and environmental magnetic application. *Geophys. J. Int.* 185, 1243–1254.

Zonneveld, K. A. F., Versteegh, G. J. M., Kasten, S., Eglinton, T. I., Emeis, K.-C., Huguet, C., Koch, B. P., de Lange, G. J., de Leeuw, J. W., Middelburg, J. J., Mollenhauer, G., Prahl, F. G., Rethemeyer, J., and Wakeham, S. G (2010): Selective preservation of organic matter in marine environments; processes and impact on the sedimentary record, *Biogeosciences*, 7, 483–511, <https://doi.org/10.5194/bg-7-483-2010>

Figure 1

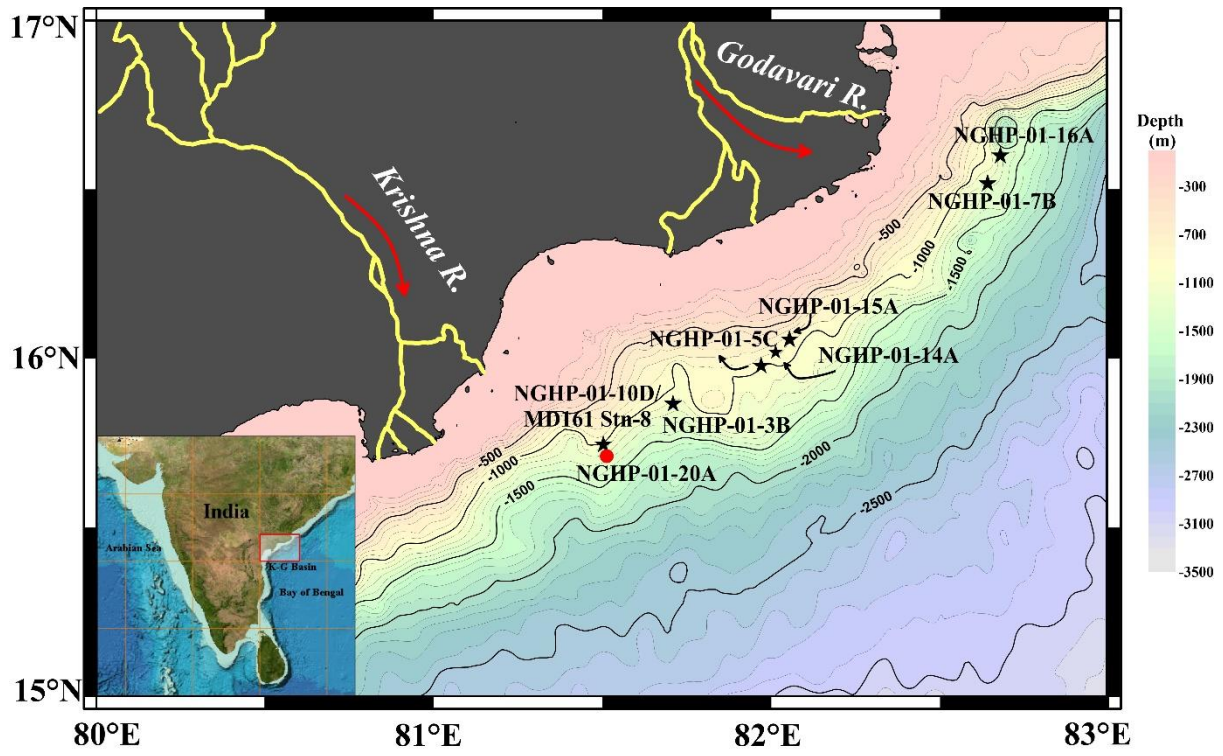


Figure 2.

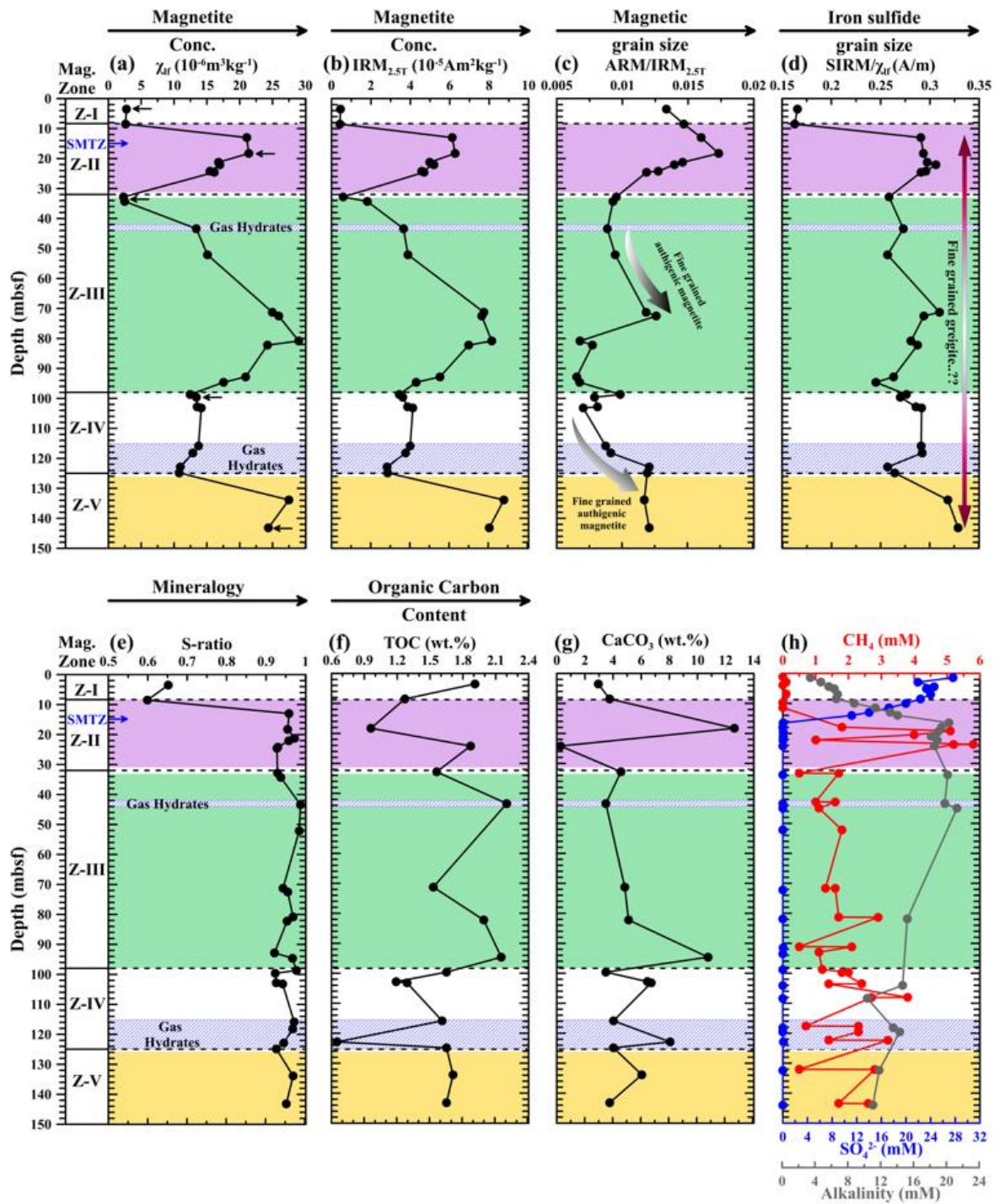


Figure 3.

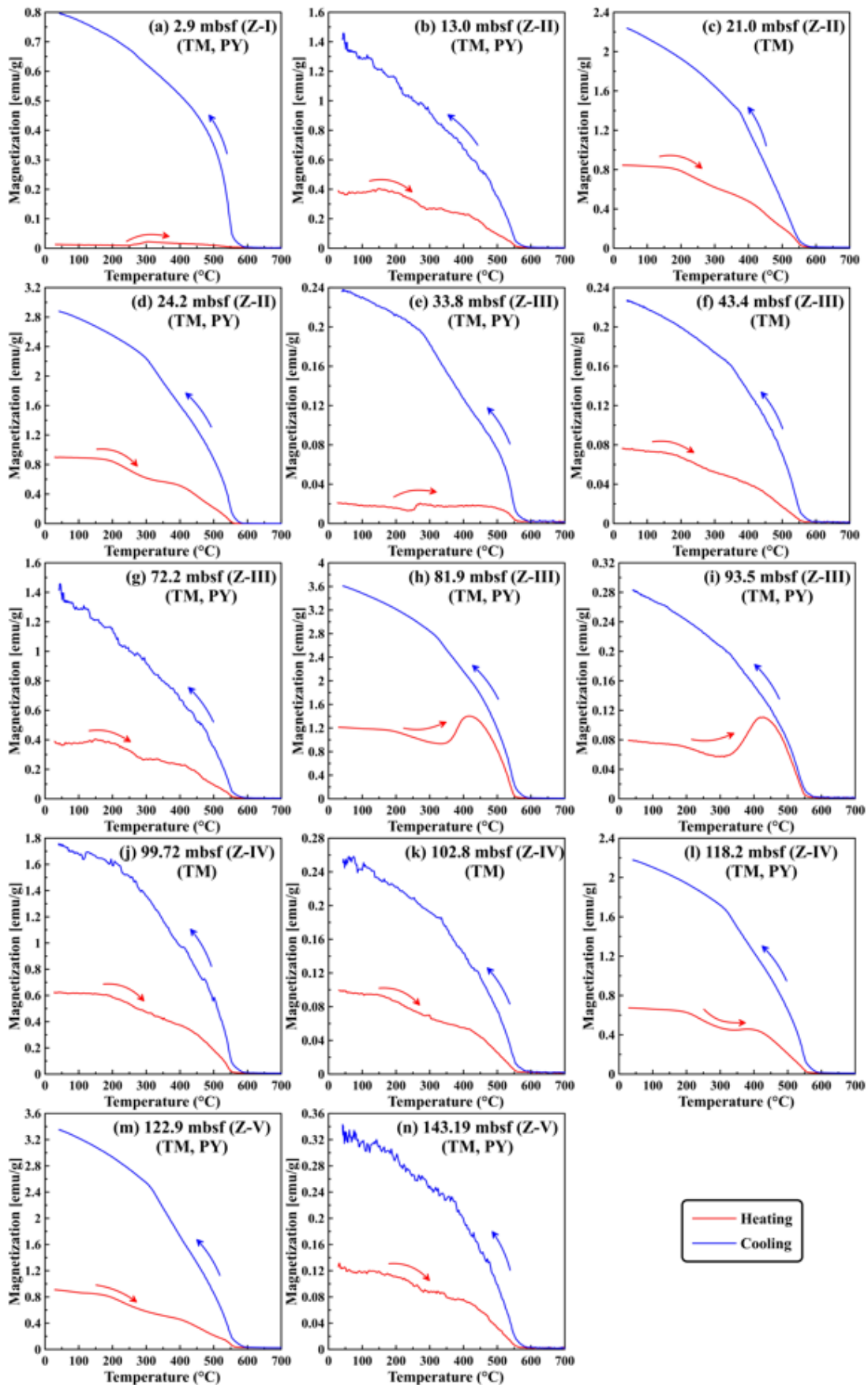


Figure 4.

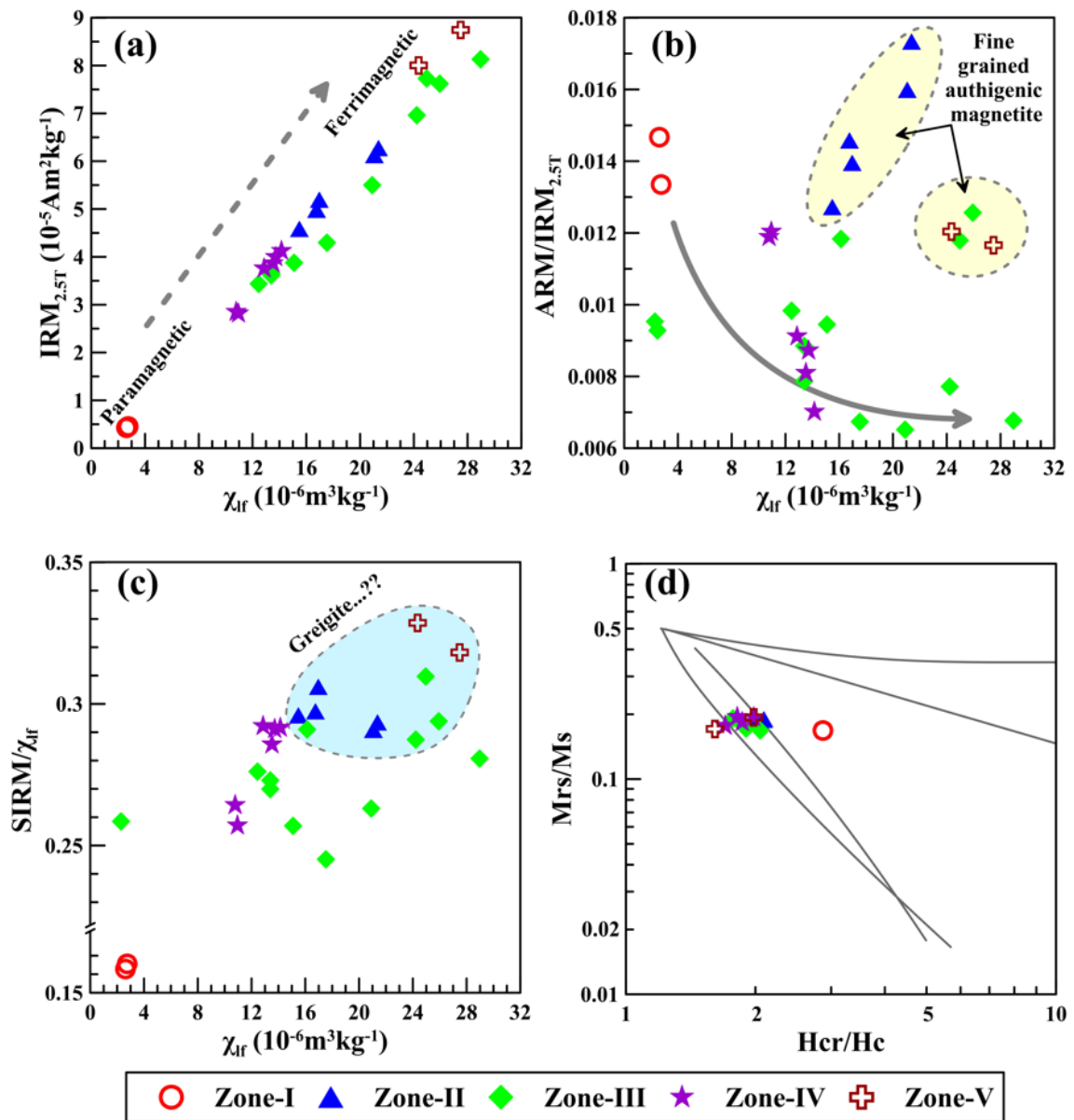


Figure 5.

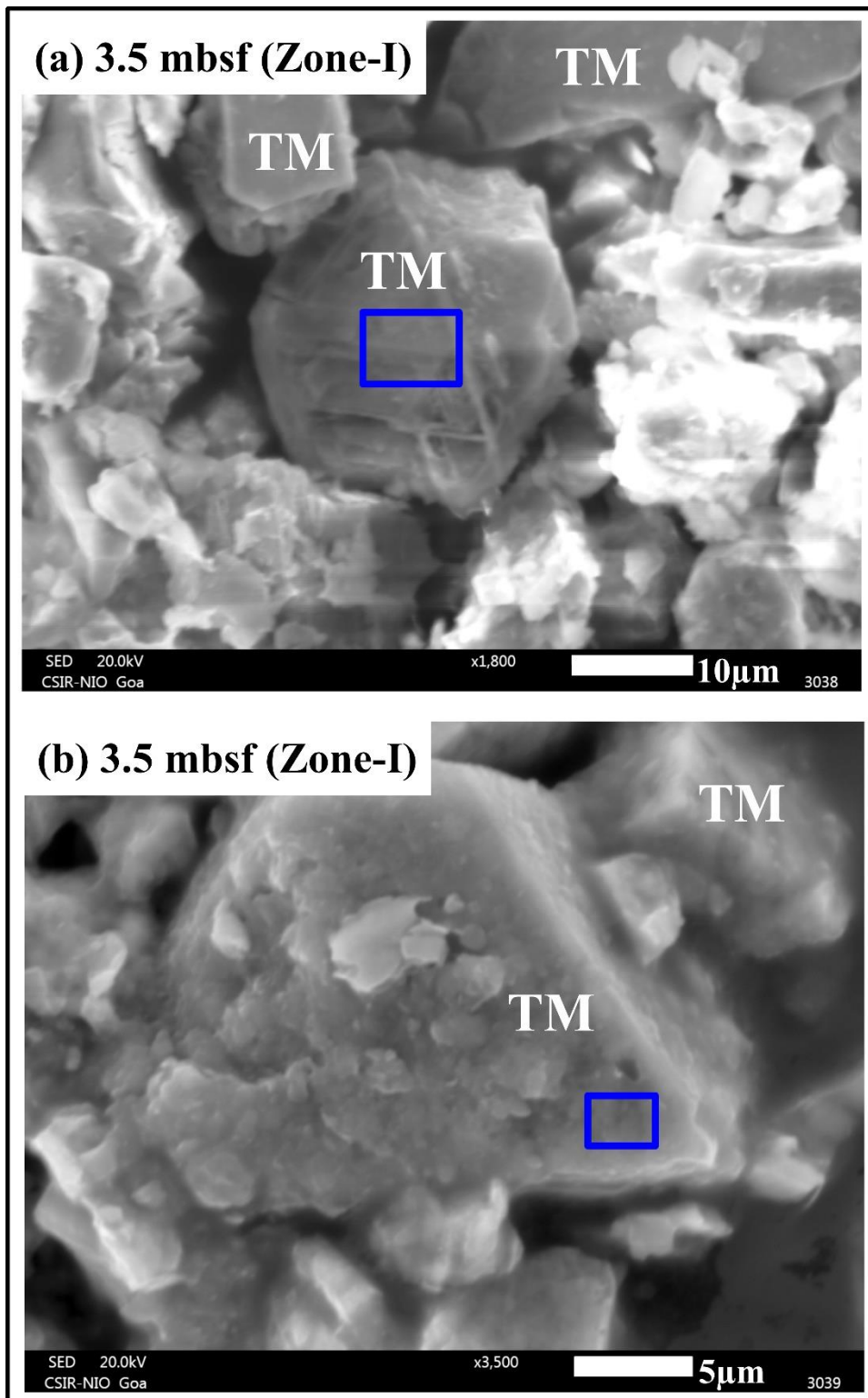


Figure 6.

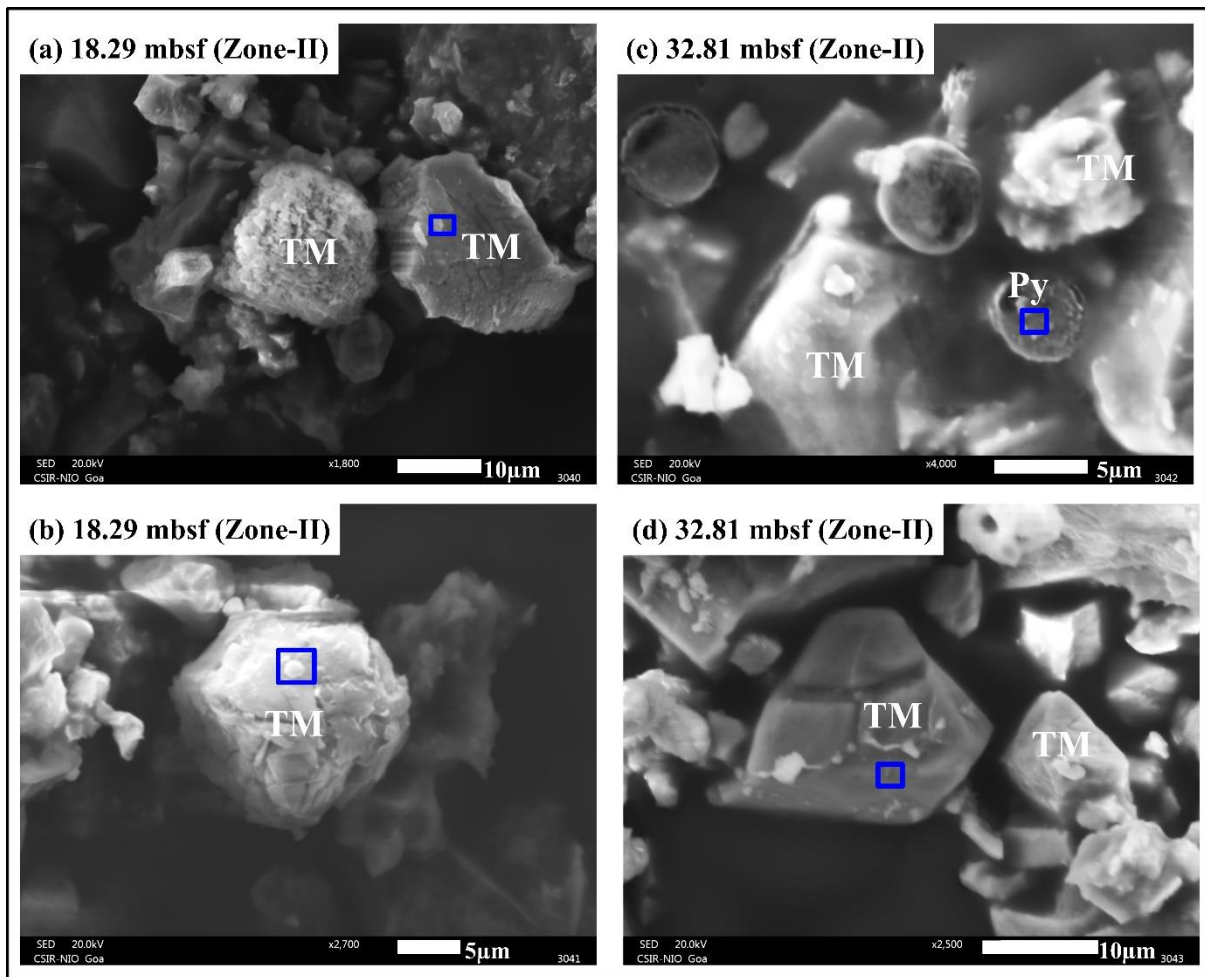


Figure 7.

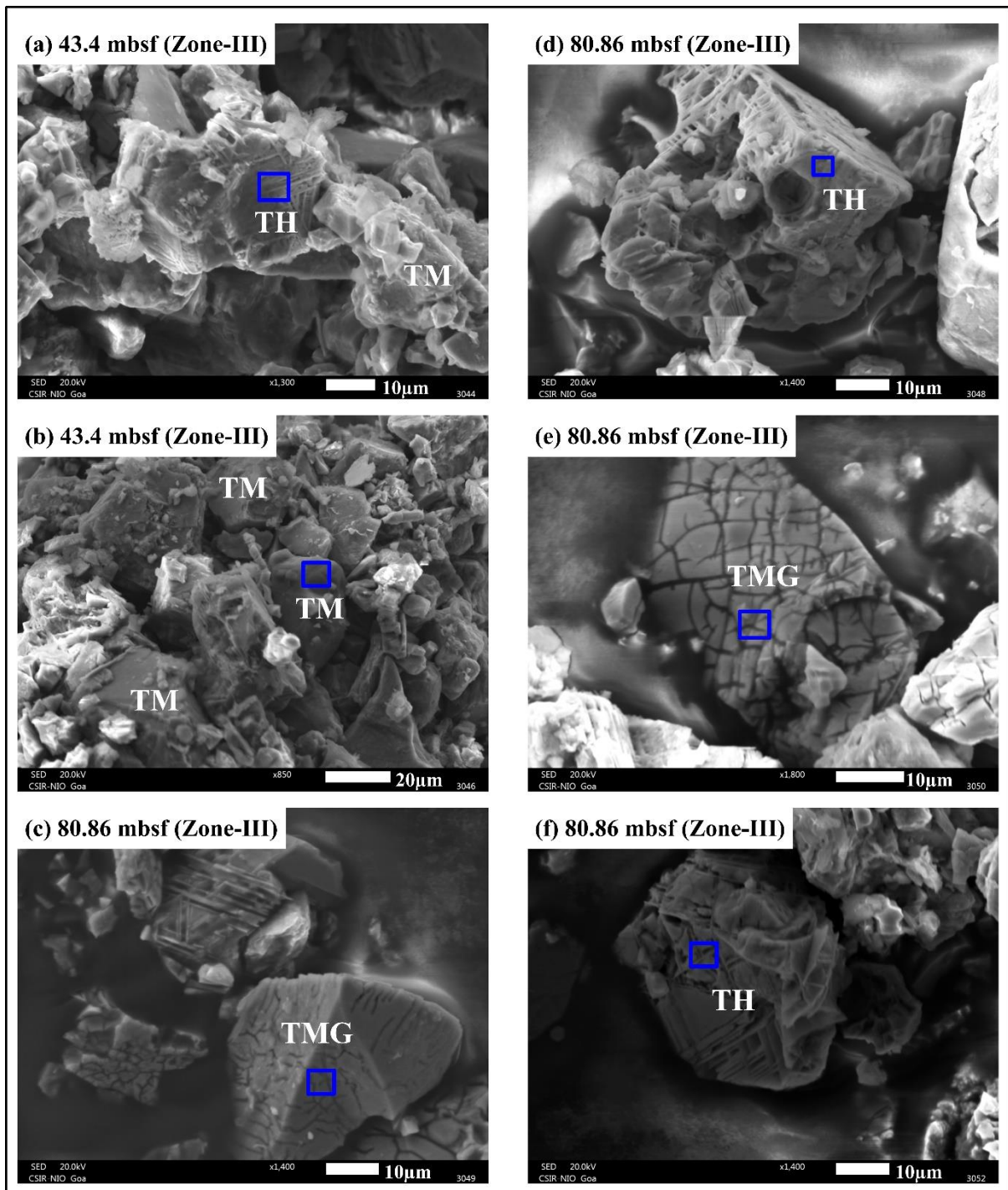


Figure 8.

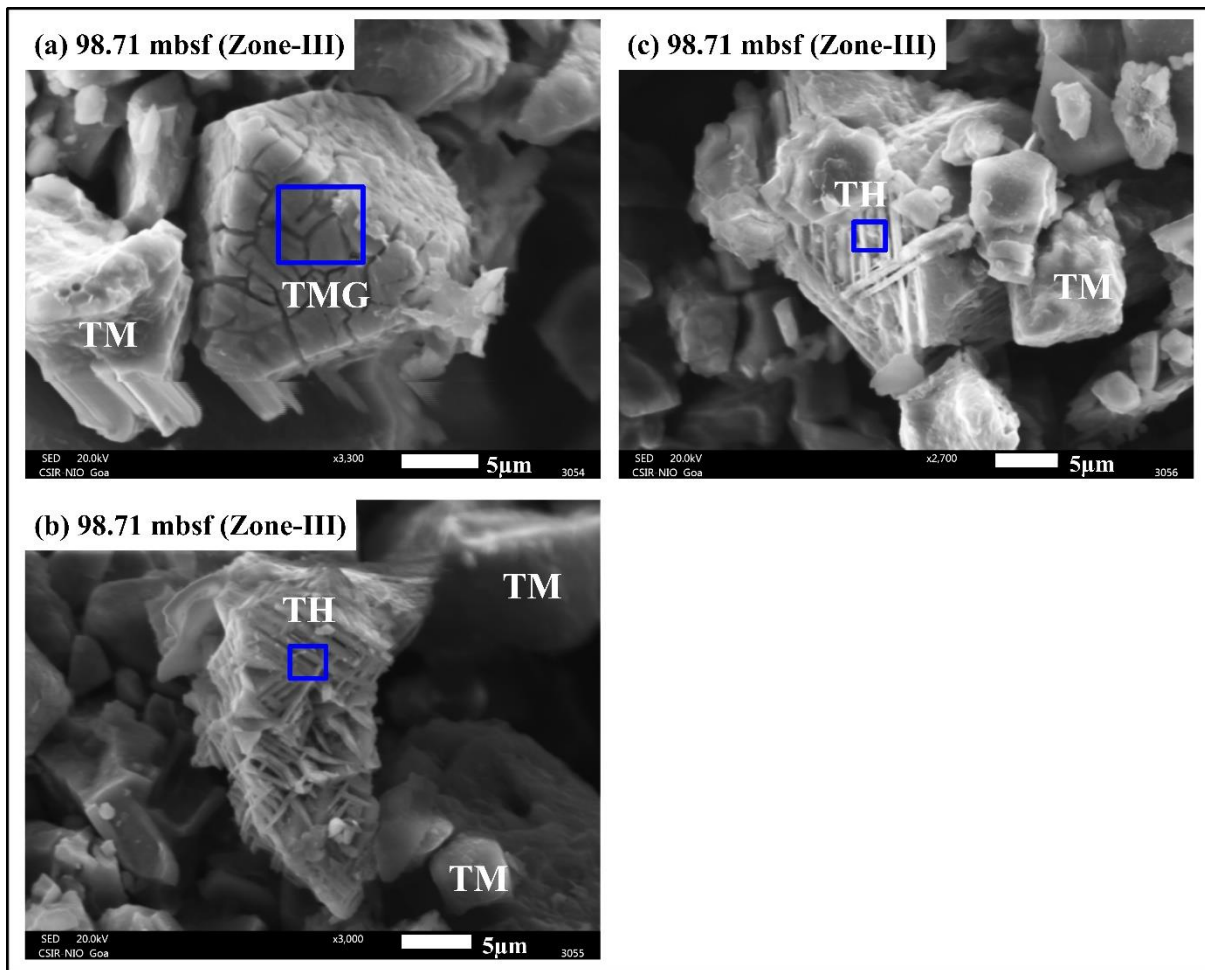


Figure 9.

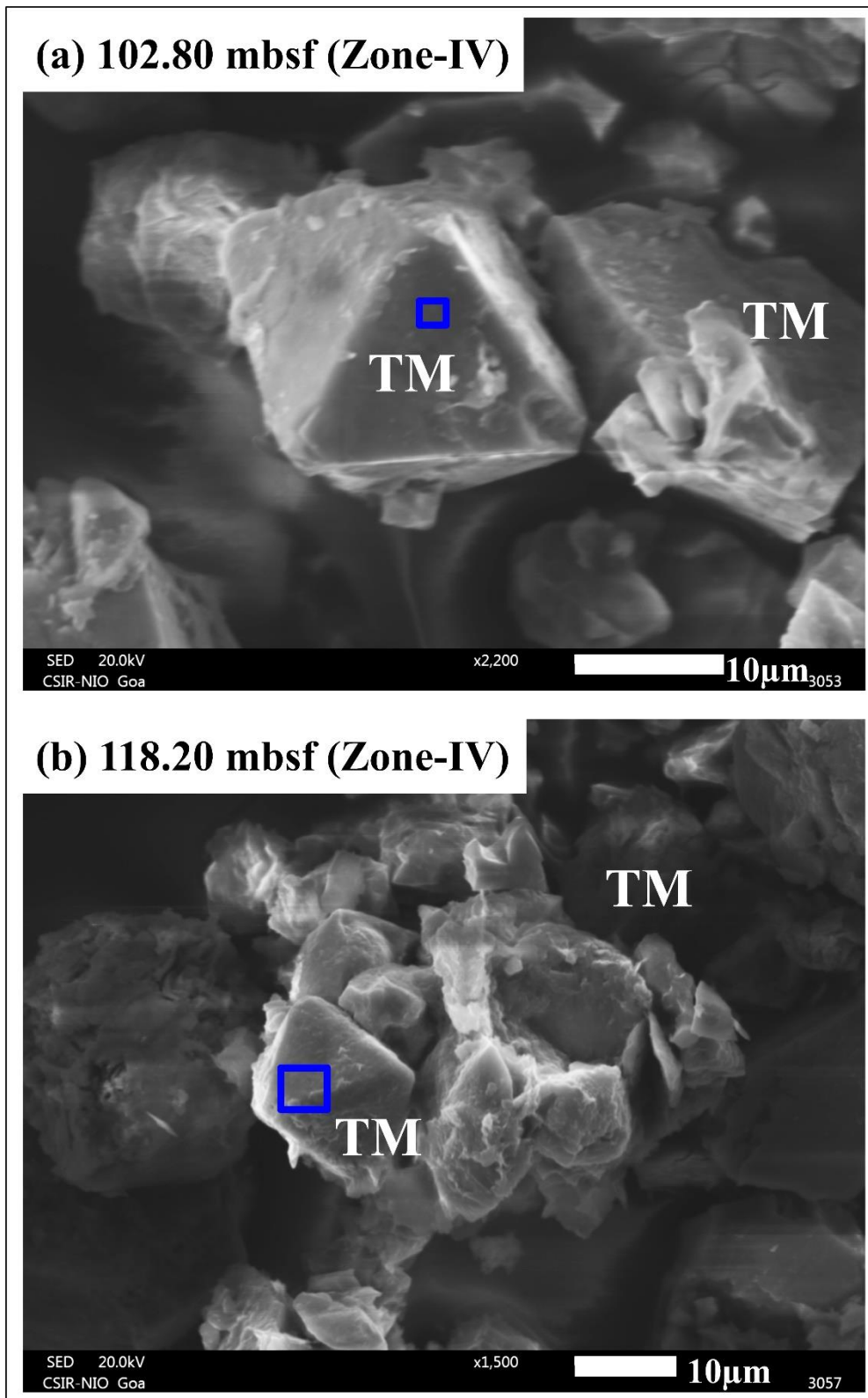


Figure 10.

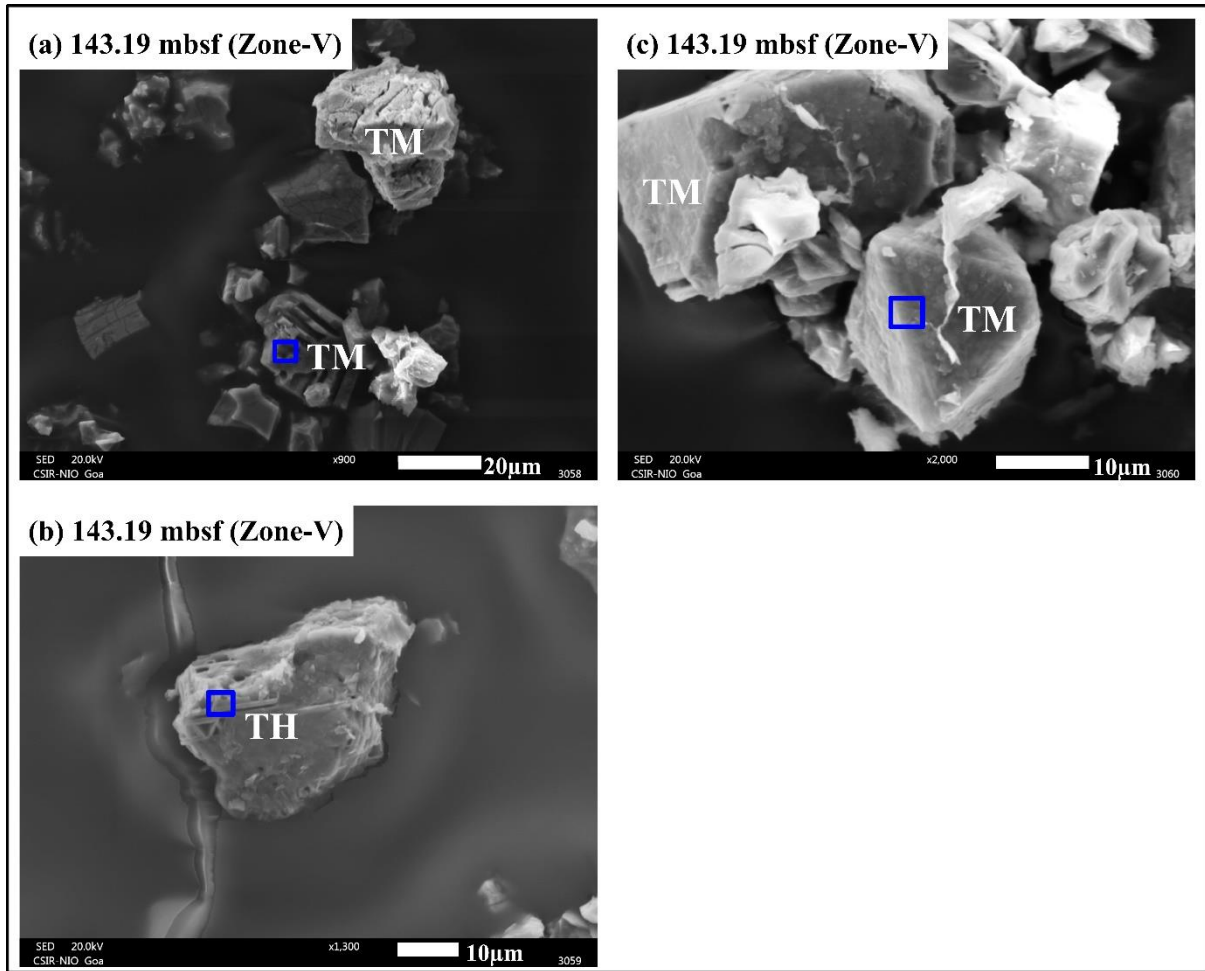


Figure 11.

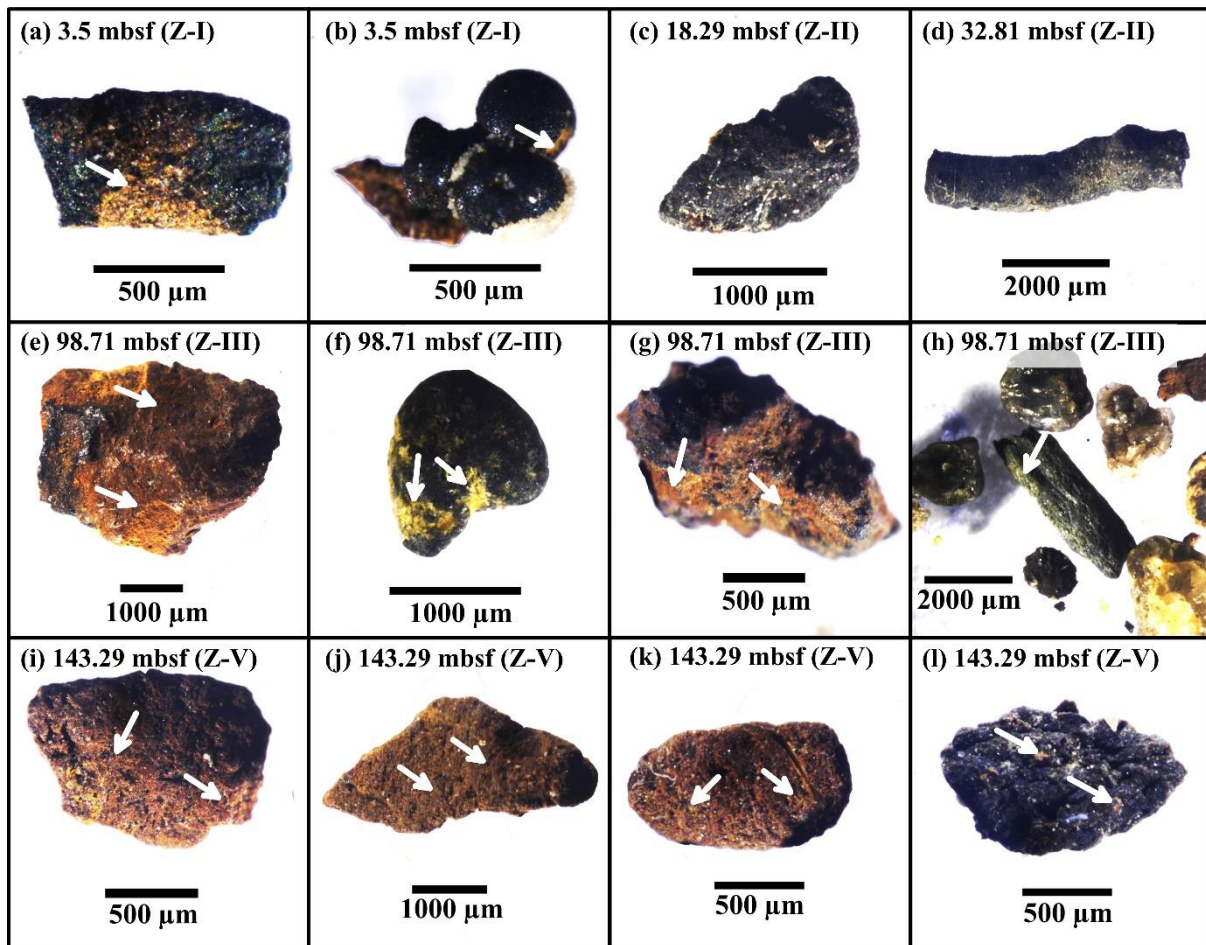


Figure 12.

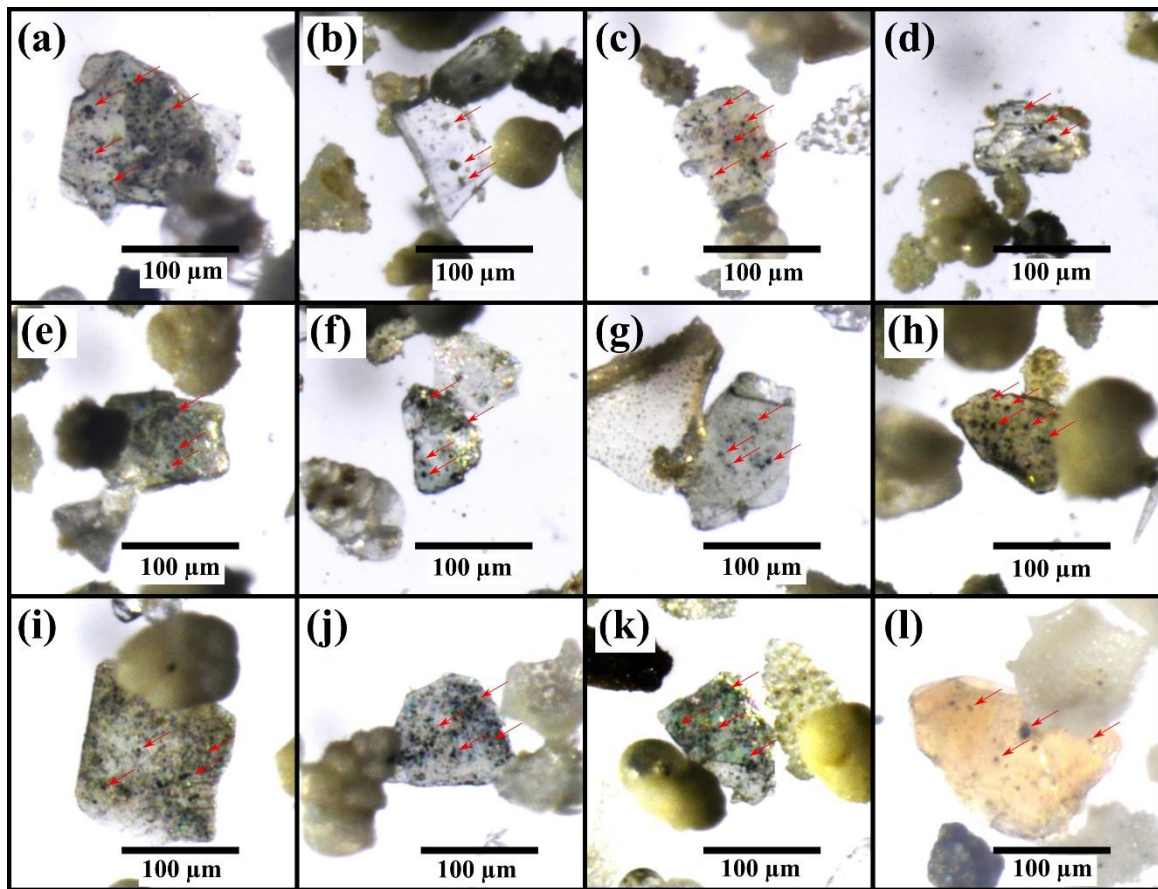


Figure 13.

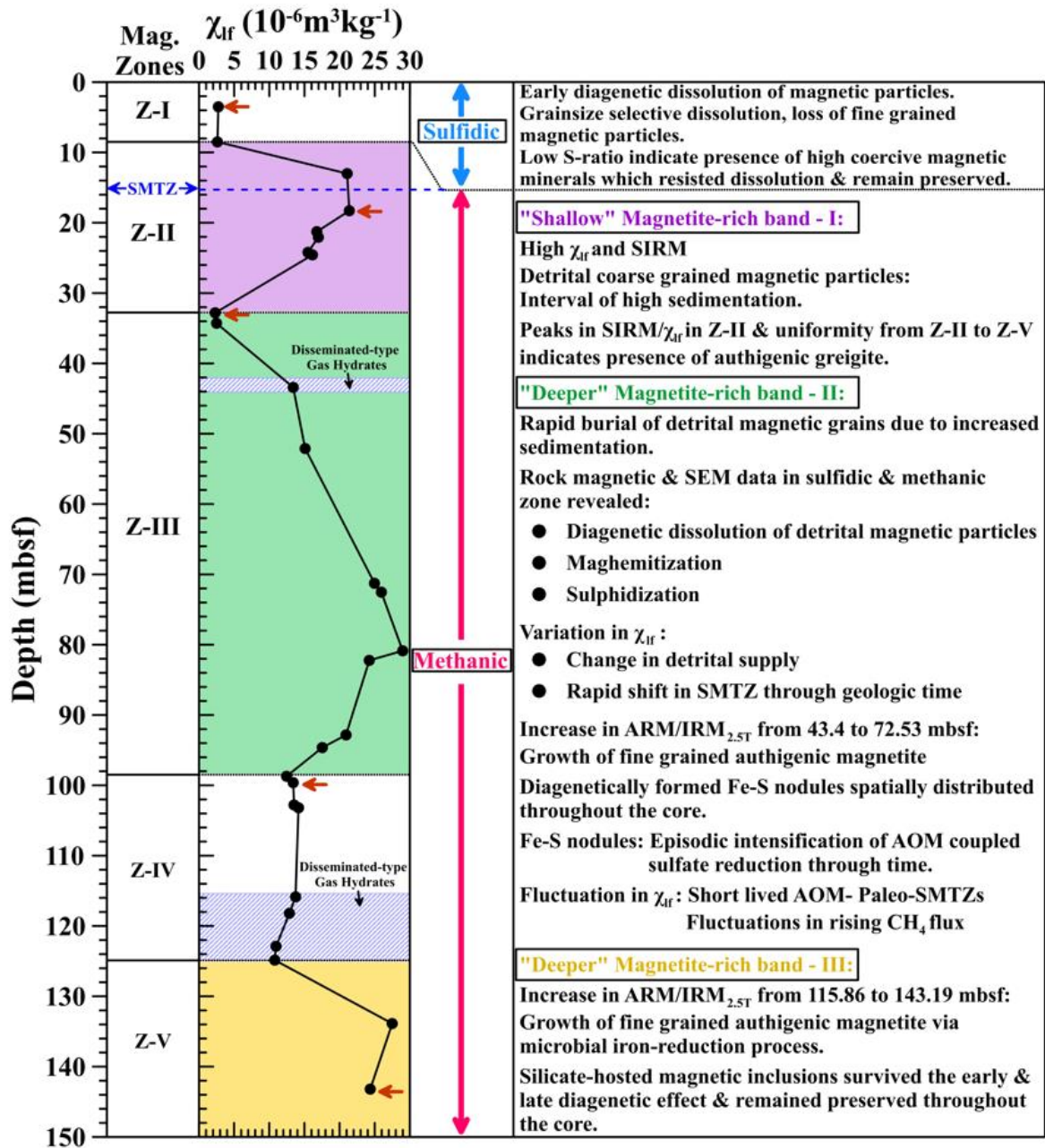


Figure S1

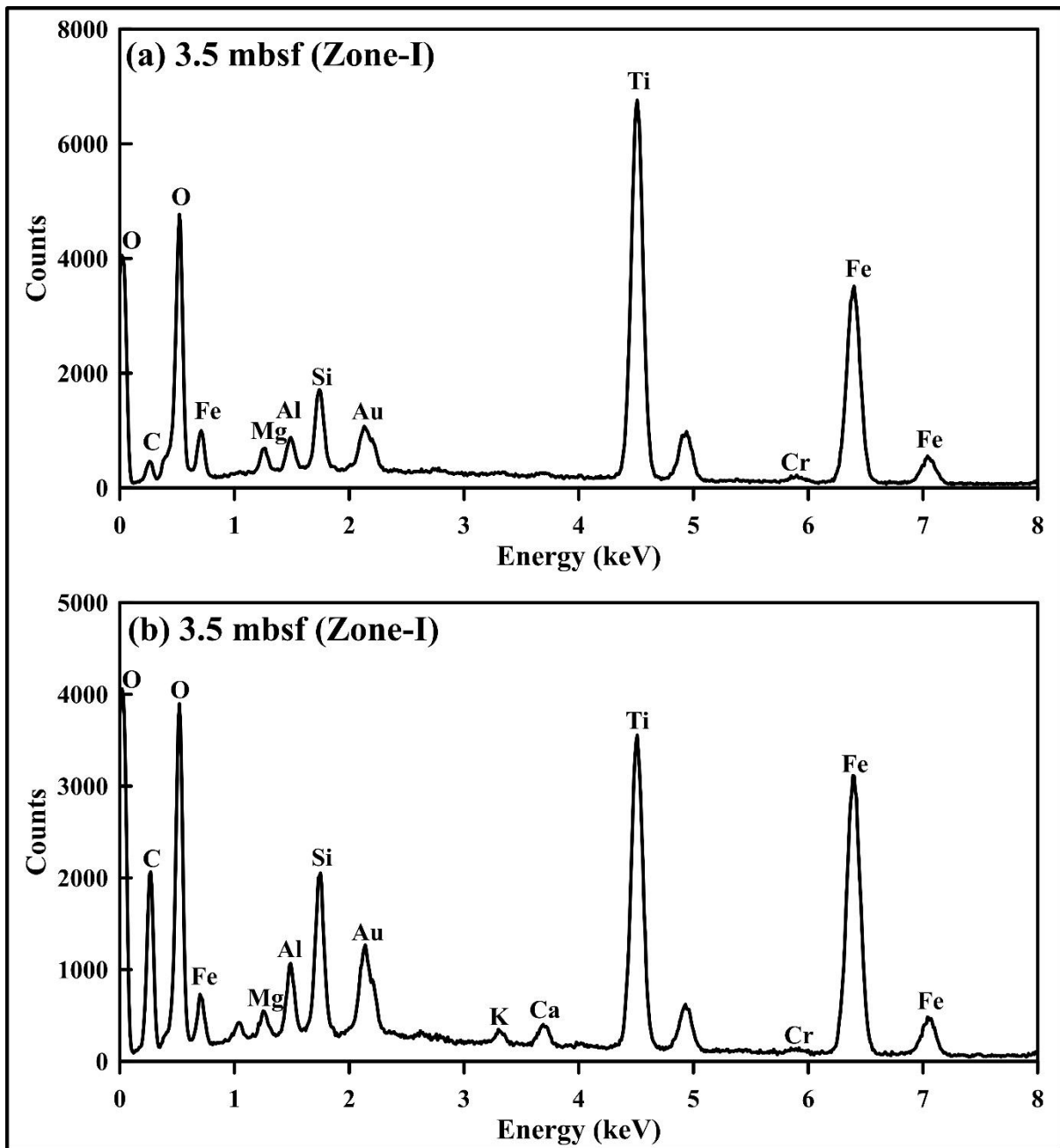


Figure S2

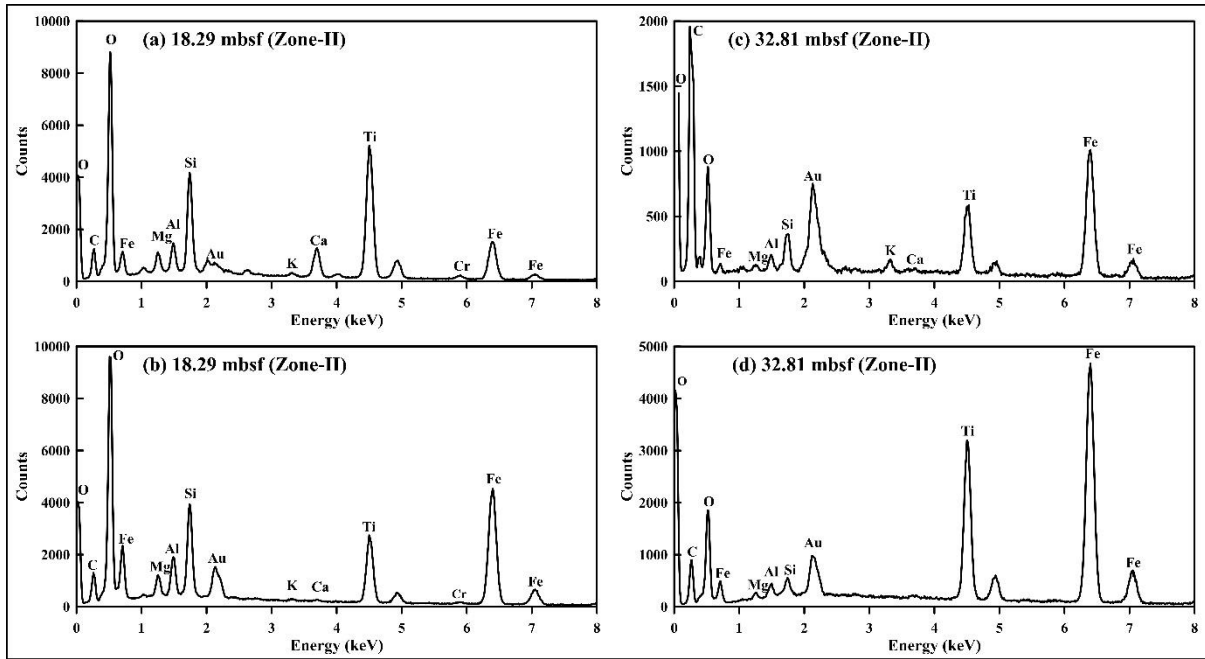


Figure S3

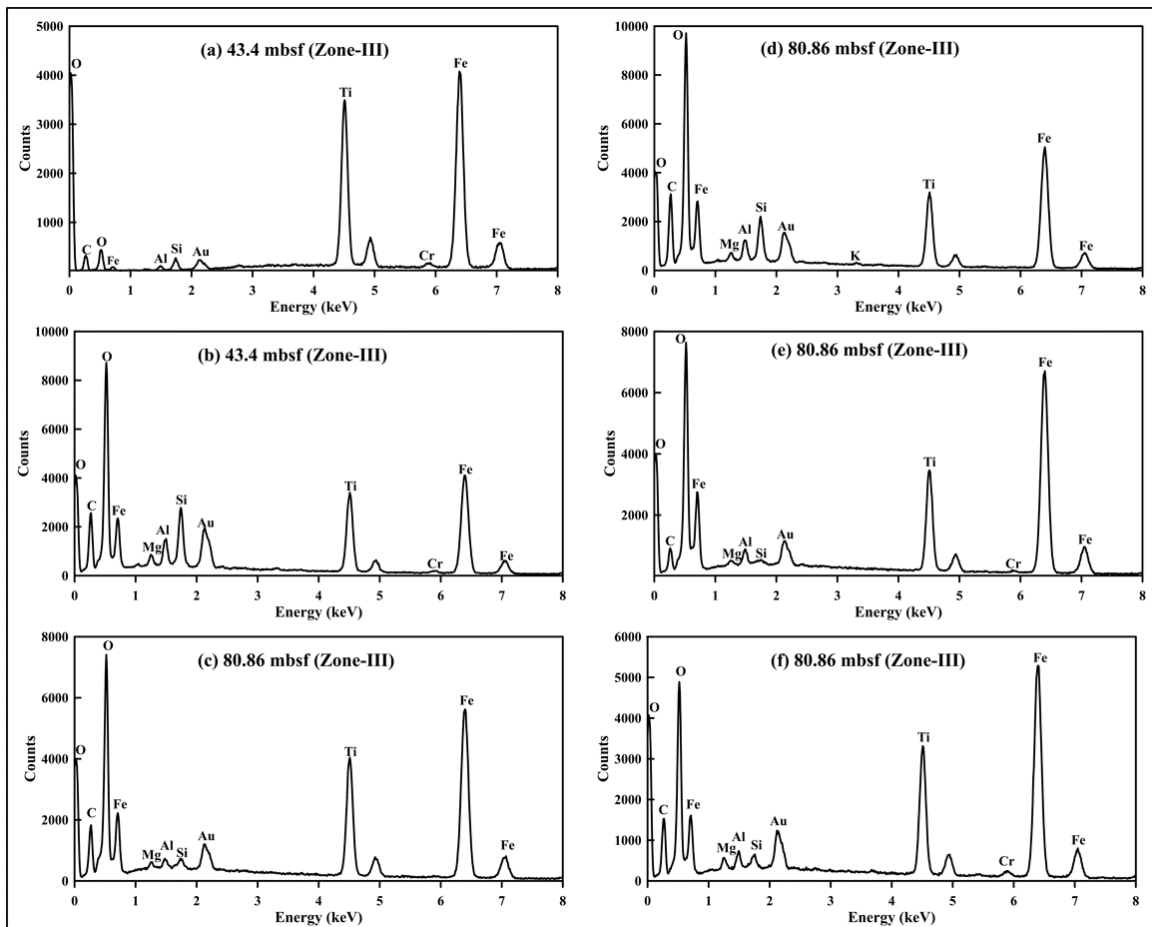


Figure S4

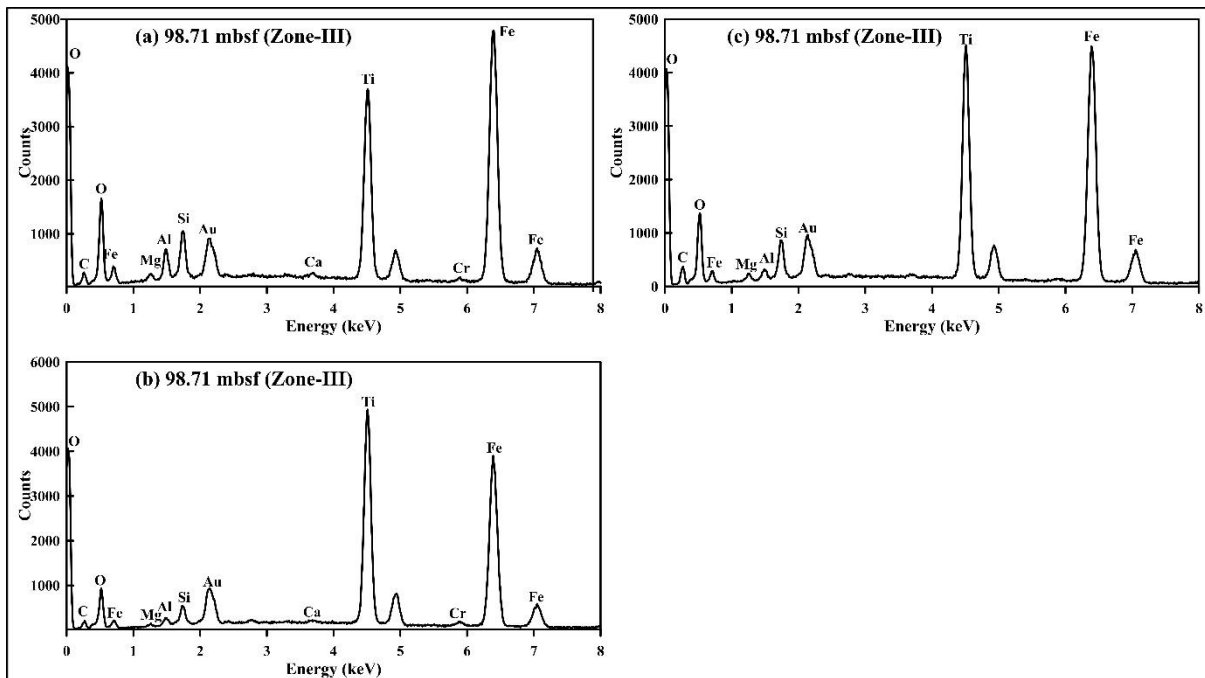


Figure S5

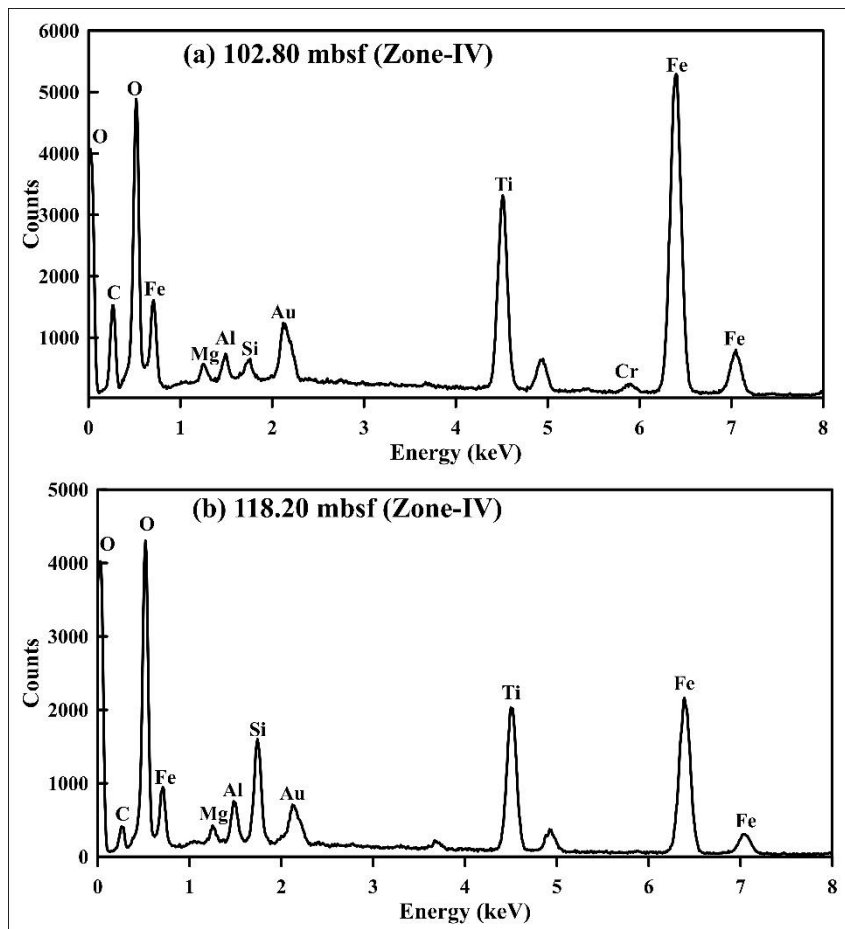


Figure S6

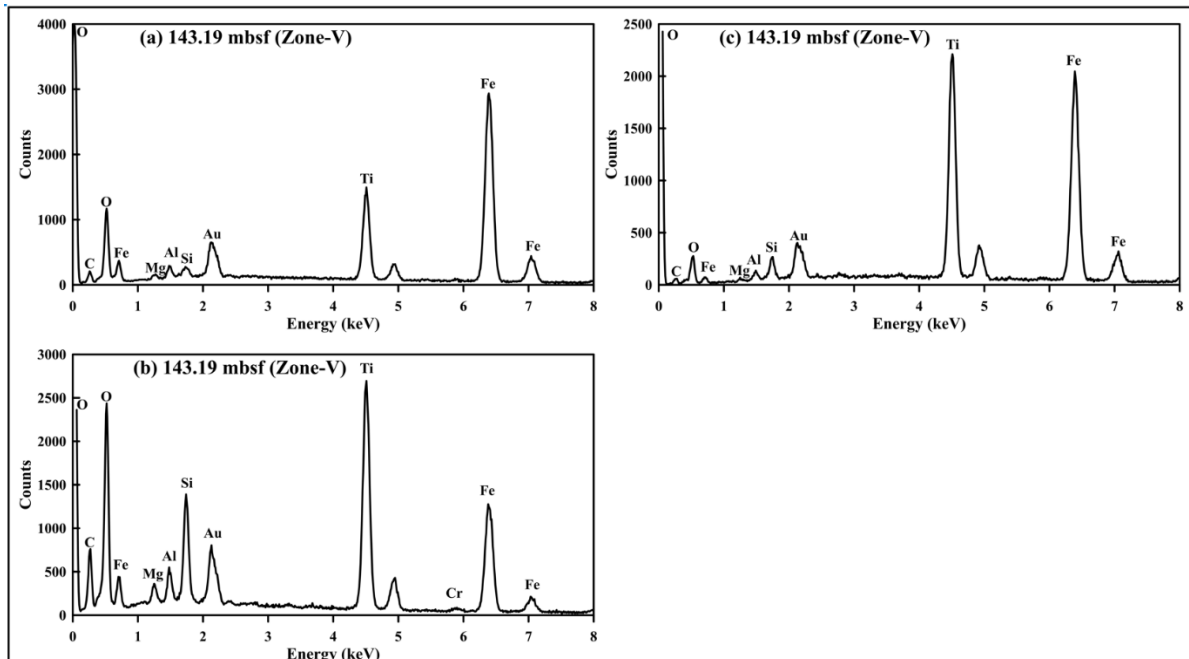


Figure S7

